Near Surface Geophysics

Re-parameterizations of the Cole-Cole model for improved spectral inversion of induced polarization data

Journal:	*Near Surface Geophysics*
Manuscript ID	nsg-2017-0014.R2
Manuscript Type:	Special Issue
Date Submitted by the Author:	n/a
Complete List of Authors:	Fiandaca, Gianluca; Aarhus University, Geoscience Meldgaard Madsen, Line; Aarhus Universitet, Geoscience Maurya, Pradip Kumar;
Keywords:	IP, Resistivity tomography, Depth of investigation

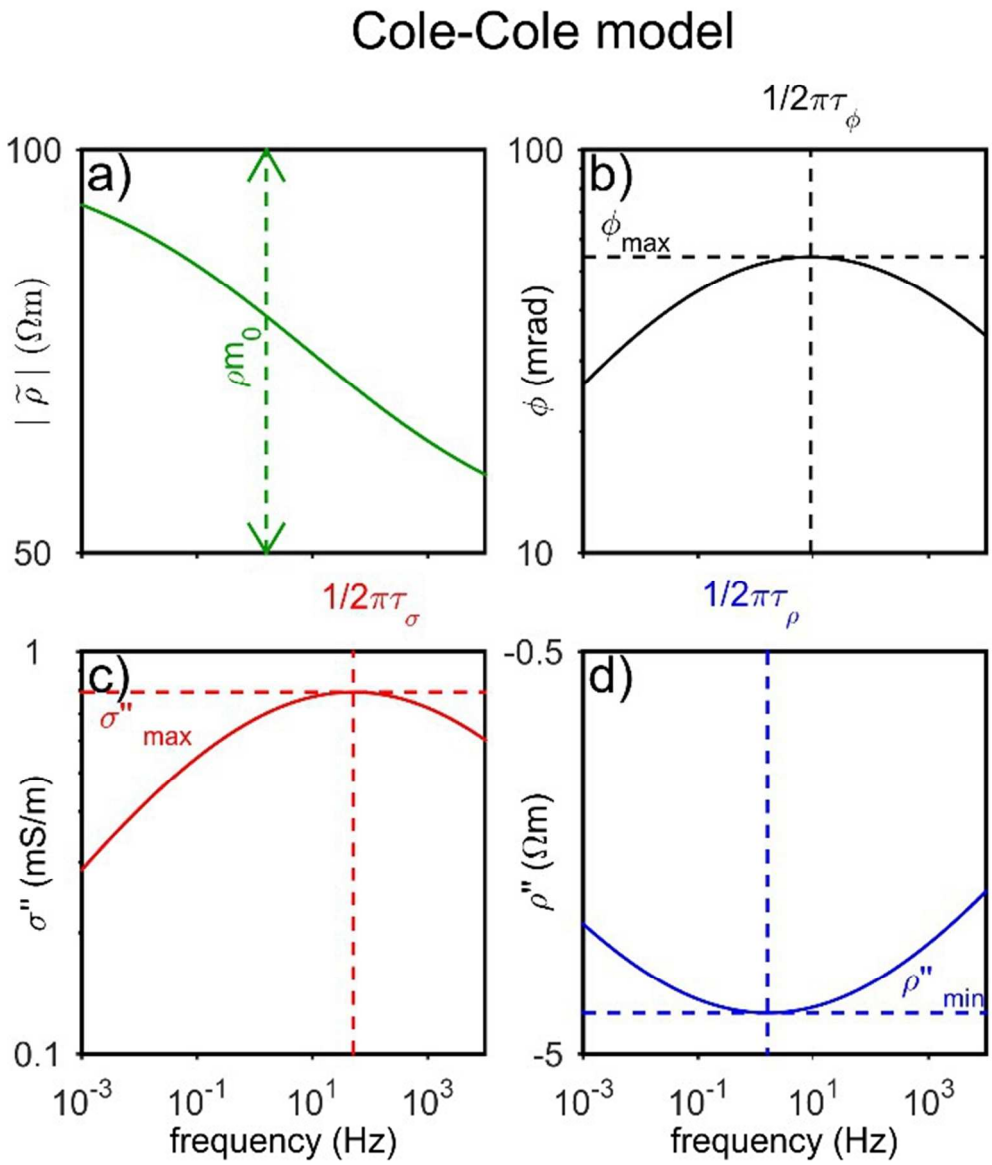

Cole-Cole model defined by ρ_0 = 100 Ωm, m_0 = 500 mV/V, τ_ρ = 0.1 s, and C = 0.2. a) amplitude of the complex resistivity; b) phase of the complex conductivity; c) imaginary conductivity; d) imaginary resistivity.

81x97mm (220 x 220 DPI)

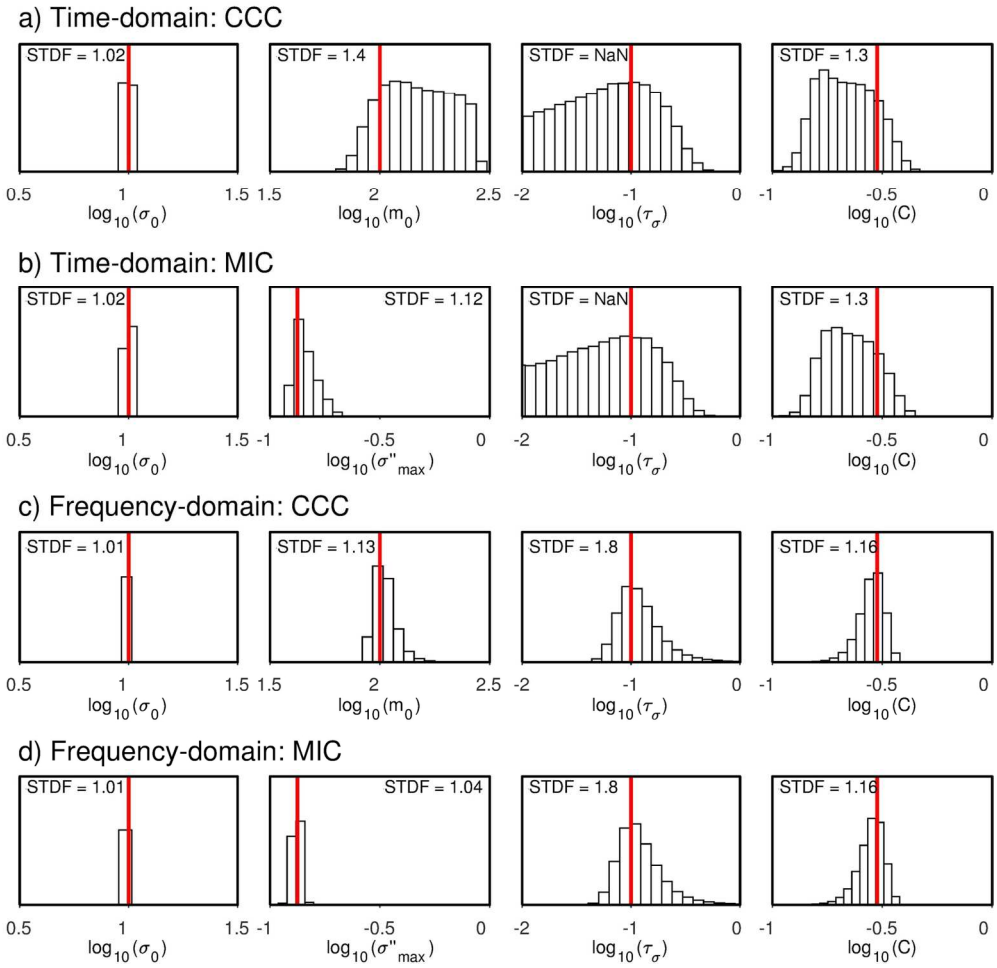

Posterior probability distributions of a homogenous half space model with the parameters: σ_0 = 10 mS/m , m_0 = 100 mV/V (σ_{max}'' = 0.13), τ_σ = 0.1 s and C = 0.3. The distributions are shown for: a) time-domain, conductivity Cole-Cole; b) time-domain, Mic Cole-Cole; c) frequency-domain, conductivity Cole-Cole; d) frequency-domain, MIC Cole-Cole. The red line marks the true model. NaN indicates that the distribution have not converged. Note that the distributions of τ_σ are wider scaled.

150x145mm (300 x 300 DPI)

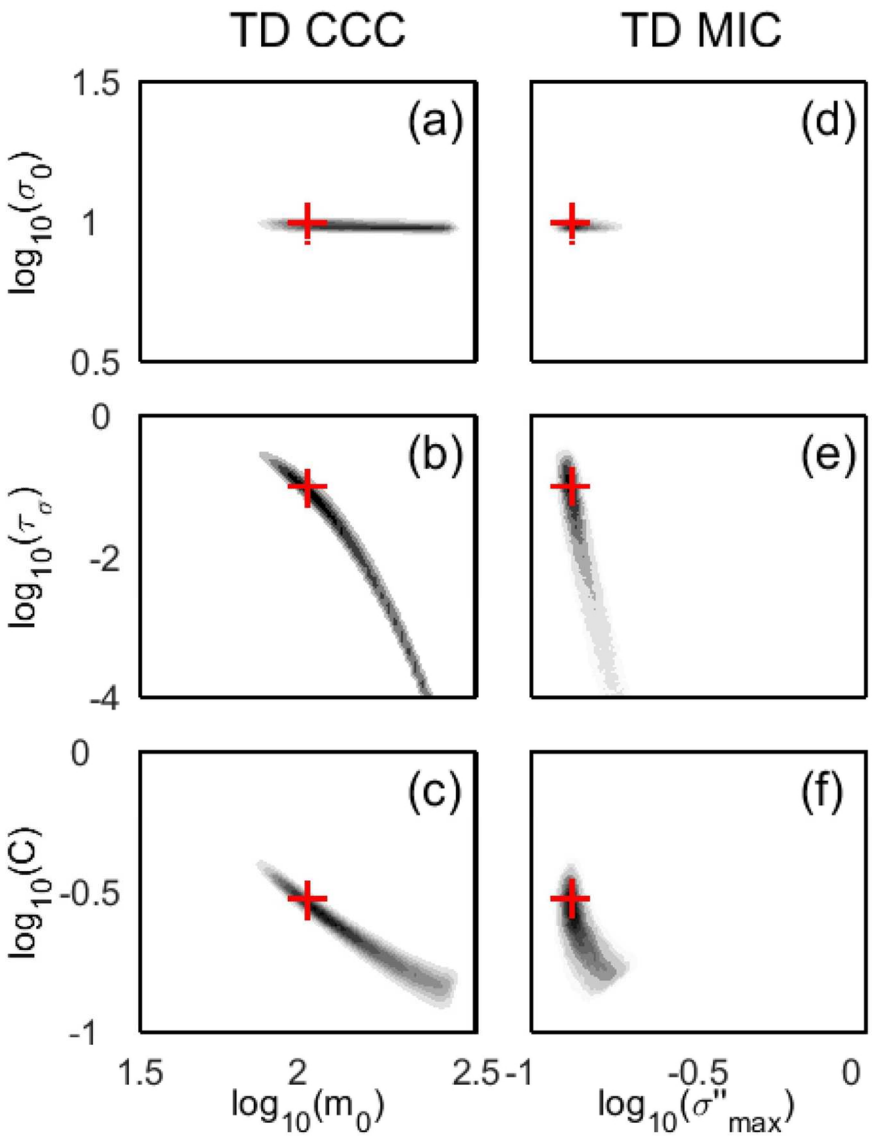

Cross-plots of the model parameters determined from inversion of time-domain data representing a homogenous half space: σ_0 = 10 mS/m m_0 = 100 mV/V (σ''_{max} = 0.13), τ_σ = 0.1 s and C = 0.3. Two different models have been used for parameterization of IP: abc) the conductivity Cole-Cole model; def) the MIC Cole-Cole model. The red cross marks the true model.

107x140mm (300 x 300 DPI)

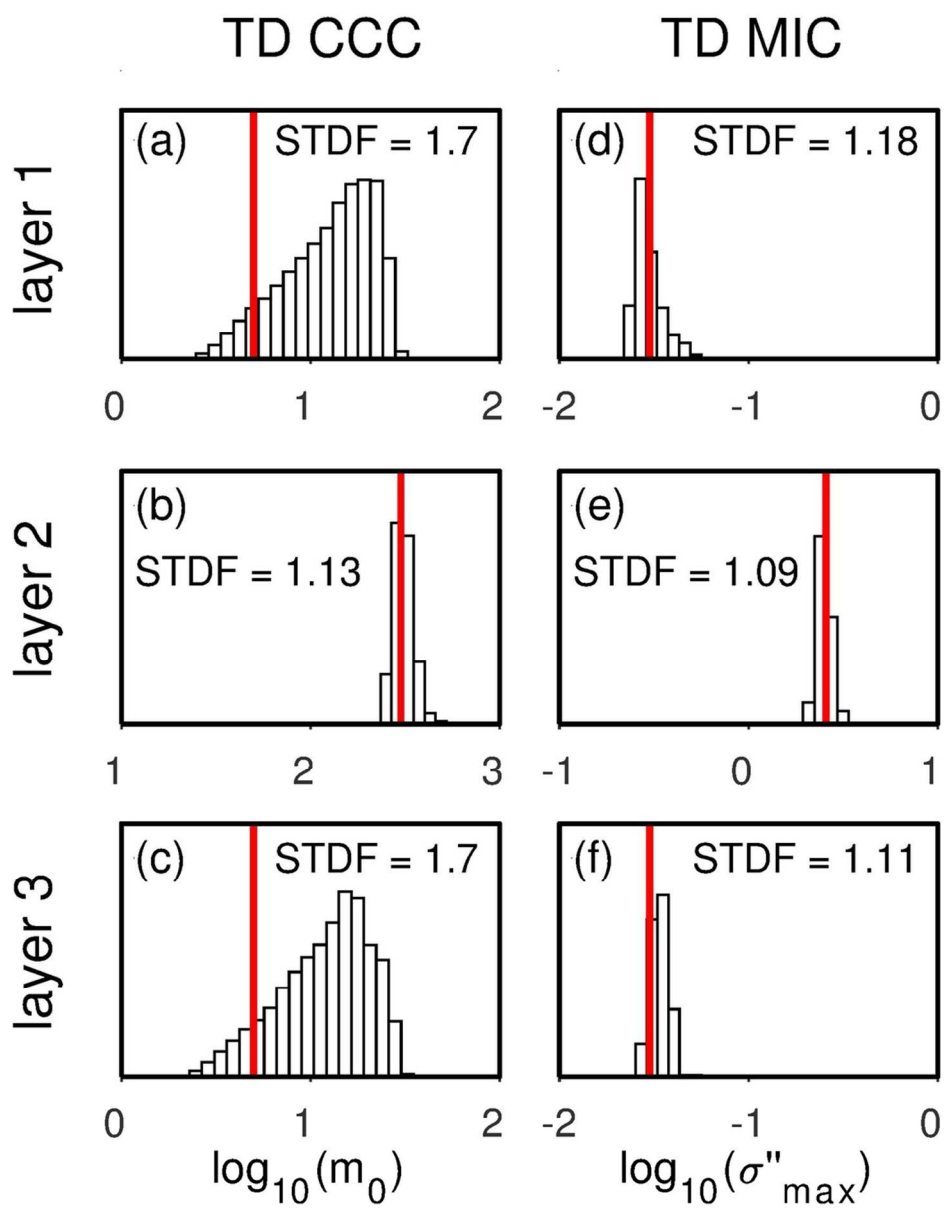

Marginal posterior probability distribution and STDFs for m_0 (the conductivity Cone-Cole model) and σ''_{max} (the MIC Cole-Cole model) for the three-layer model specified in the text. The red line marks the true model values.

95x123mm (300 x 300 DPI)

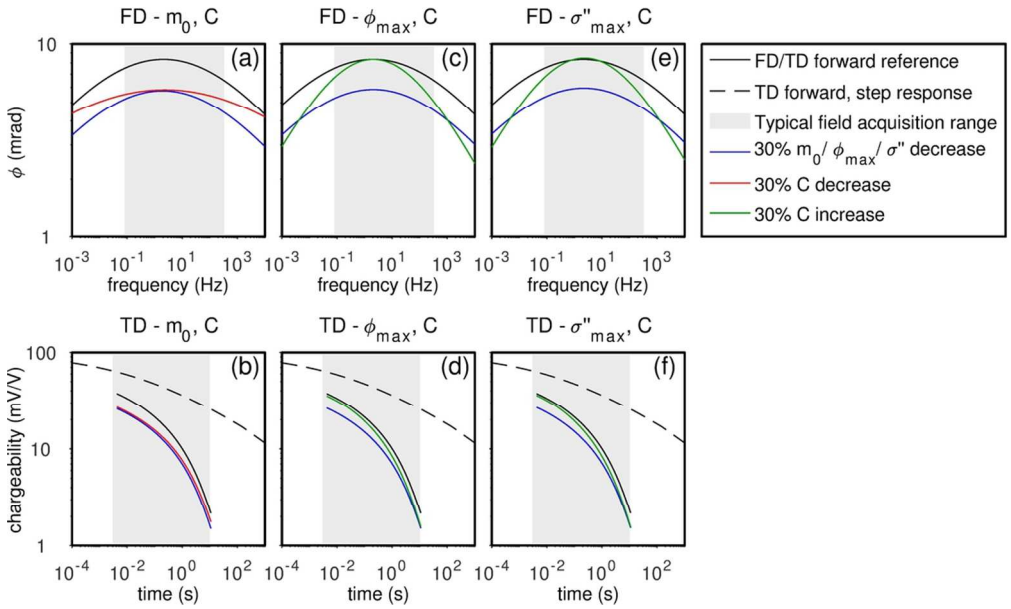

Variations of frequency-domain (FD) and time-domain (TD) responses with m_0,φ_max,σ_max^'' and C. Reference model: ρ_0=100 Ωm, m_0=100 mV/V, τ_ρ=0.1 s, and C=0.2. a) FD responses, m_0 and C variations; b) TD responses, m_0 and C variations; c) FD responses, φ_max and C variations; d) TD responses, φ_max and C variations; e) FD responses, σ_max^'' and C variations; f) TD responses, σ_max^'' and C variations.

102x60mm (300 x 300 DPI)

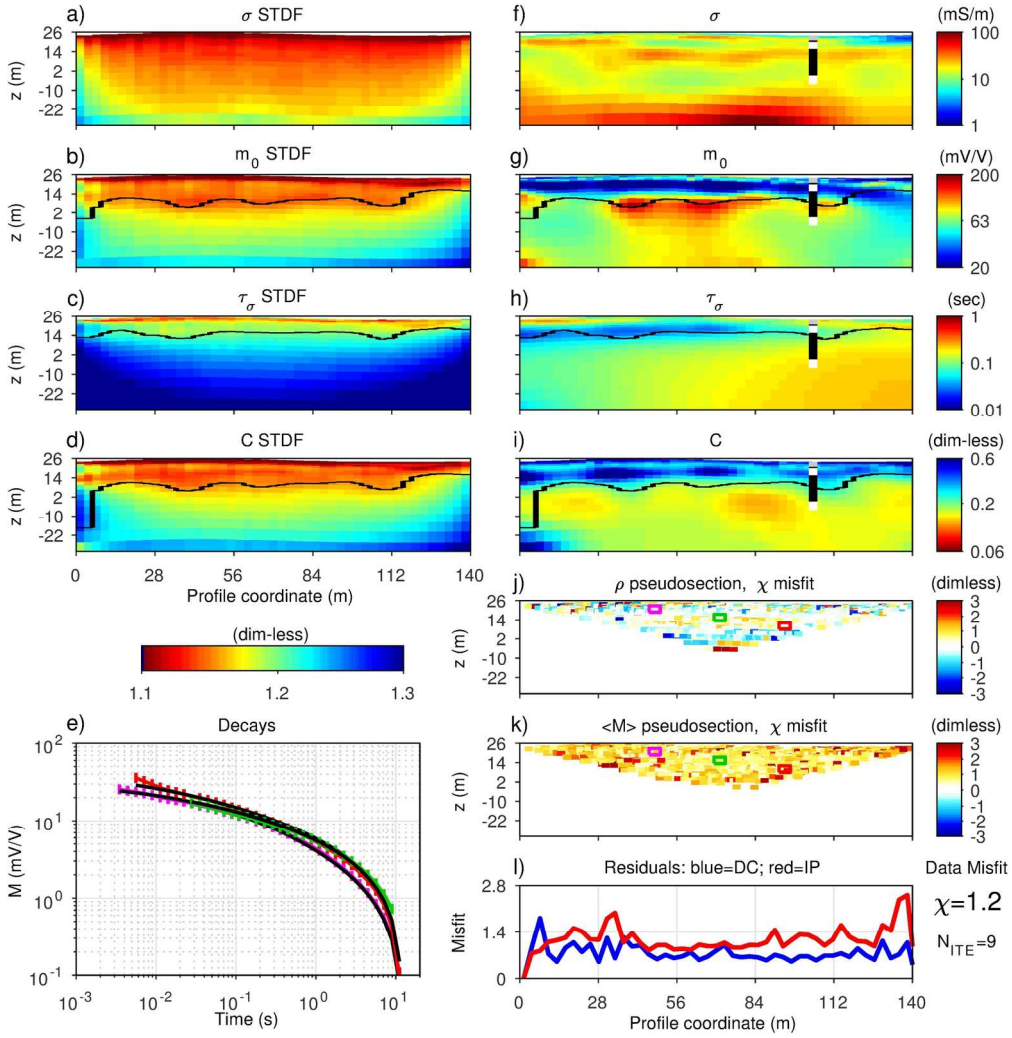

Inversion model, uncertainty analysis and misfit of field data from Samsø, Denmark, obtained using the conductivity Cole-Cole parameterization. a-d) the uncertainty analysis given as the STDF of the four model parameters; e) three examples of IP decays with error bars (the locations of the data cells are marked in panel j and k) and fitting forward response (black lines); f -i) inversion model with borehole information (white is sand, black is till and grey is silt); j) resistivity pseudosection showing the misfit χ; k) pseudosection of the root mean square χ for the entire IP decay (defined positive). l) misfit of DC (blue) and IP (red) data of the inversion averaged vertically (and over all gates for the IP misfit) along the pseudosection. N_ITE is the number of iterations. The black lines in panel a-d and f-i are the DOI.

166x171mm (300 x 300 DPI)

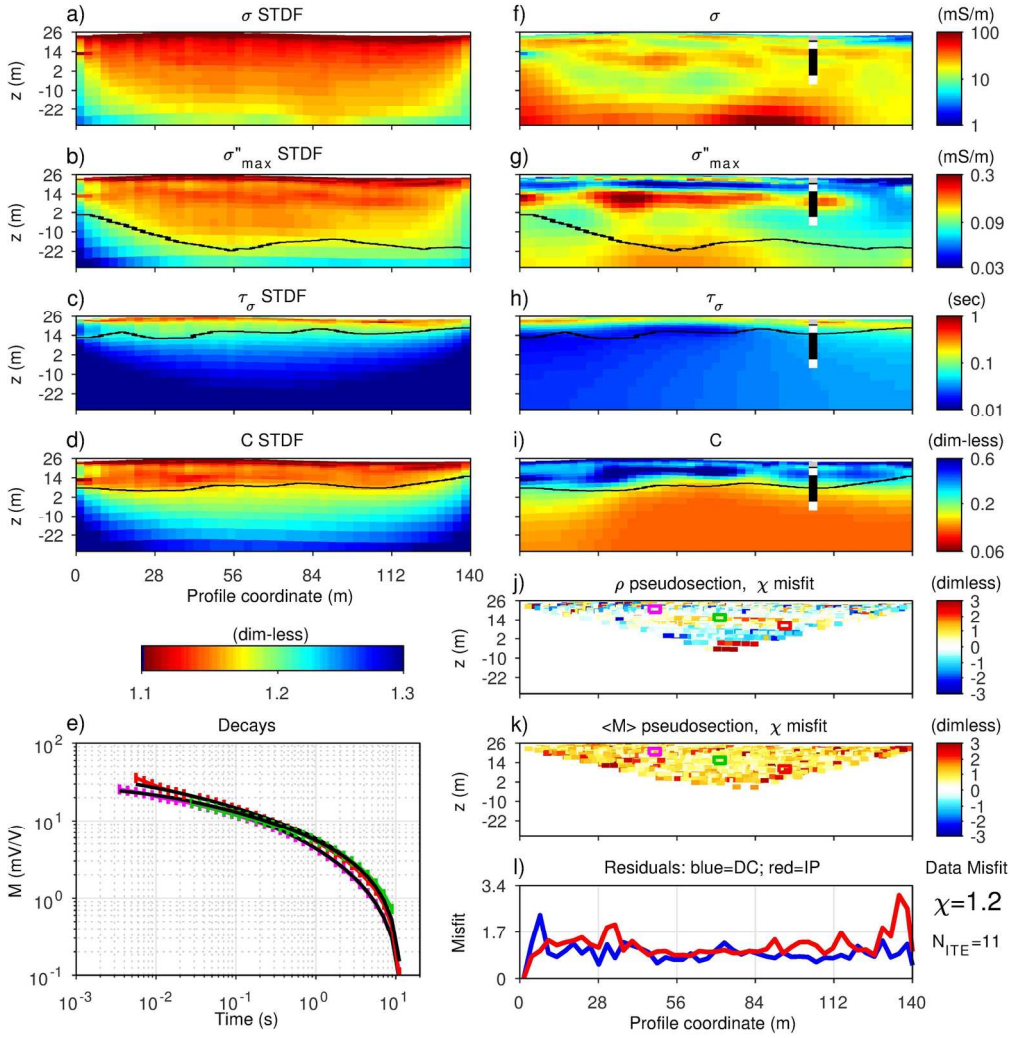

Inversion model, uncertainty analysis and misfit of field data from Samsø, Denmark, obtained using the MIC Cole-Cole model for parameterization of IP. a-d) the uncertainty analysis given as the STDF of the four model parameters; e) three examples of IP decays with error bars (the locations of the data cells are marked in panel j and k) and fitting forward response (black lines); f -i) inversion model with borehole information (white is sand, black is till and grey is silt); j) resistivity pseudosection showing the misfit χ; k) pseudosection of the root mean square χ for the entire IP decay (defined positive). l) misfit of DC (blue) and IP (red) data of the inversion averaged vertically (and over all gates for the IP misfit) along the pseudosection. N_ITE is the number of iterations. The black lines in panel a-d and f-i are the DOI.

166x171mm (300 x 300 DPI)

Re-parameterizations of the Cole-Cole model for improved spectral inversion of induced polarization data

Gianluca Fiandaca*, Line Meldgaard Madsen*, Pradip Kumar Maurya*

*HydroGeophysics Group, Department of Geoscience, Aarhus University,

C.F. Møllers Alle 4, DK-8000 Aarhus C, Denmark

Short title: Re-parameterization of Cole-Cole model

Date of first submission: 31.01.2017

Resubmission: 20.09.2017

Corresponding author: Line Meldgaard Madsen, linemeldgaad@geo.au.dk

ABSTRACT

The induced polarization phenomenon, both in time-domain (TD) and frequency-domain (FD), is often parameterized using the empirical Cole-Cole model. To improve the resolution of model parameters and to decrease the parameter correlations in the inversion process of induced polarization data, we here suggest three re-parametrizations of the Cole-Cole model, namely the Maximum Phase Angle (MPA) Cole-Cole model, the Maximum Imaginary Conductivity (MIC) Cole-Cole model and the Minimum Imaginary Resistivity (MIR) Cole-Cole model. The MPA Cole-Cole model uses the maximum phase φ_{max} and the inverse of the phase peak frequency, τ_{φ}, instead of the intrinsic chargeability m_0 and the time constant adopted in the classic Cole-Cole model; the MIC Cole-Cole model uses the maximum imaginary conductivity σ''_{max} instead of the m_0, and the time constant τ_{σ} of the Cole-Cole model in its conductivity form; the MIR Cole-Cole model uses the minimum imaginary resistivity ρ''_{min} instead of the m_0, and the time constant τ_{ρ} of the Cole-Cole model in its resistivity form.

The effects of the three re-parameterizations have been tested on synthetic TD and FD data using a Markov Chain Monte Carlo inversion method, which allows for easy quantification of parameter uncertainty, and on field data using 2D gradient-based inversion. In comparison with the classic Cole-Cole model, it was found that for all the three re-parameterizations the model parameters are less correlated with each other and, consequently, better resolved for both TD and FD data. The increase in model resolution is particularly significant for models that are poorly resolved using the classic Cole-Cole parameterization, for instance for low values of the frequency exponent or with

EAGE Publications B.V., PO Box 59, 3990 DB, Houten, The Netherlands

low signal-to-noise ratio. In general, this leads to a significantly deeper depth of investigation for the φ_{max}, σ''_{max} and ρ''_{min} parameters, when compared to the classic m_0 parameter, which is shown with a field example. We believe that the use of the re-parameterizations for inverting field data will contribute to narrow the gap between IP theory, laboratory findings and field applications.

INTRODUCTION

The induced polarization (IP) method is a geophysical technique providing direct sensitivity to the electrical properties of the subsurface at the interface between the rock matrix and the wetting fluid. The method was originally used for mineral exploration, but, today, it is frequently applied in environmental surveys where the applications include mapping and characterization of lithology and soil-types (e.g. Slater and Lesmes, 2002, Kemna et al., 2004, Maurya et al., 2016, Johansson et al., 2016) and characterization of contaminated sites and landfills (e.g. Vanhala, 1997, Leroux et al., 2007, Gazoty et al., 2012, Johansson et al., 2015). Studies have also been investigating the link between the IP effect and hydraulic properties of the subsurface (e.g. Börner et al., 1996, Binley et al., 2005, Weller et al., 2015, Nordsiek et al., 2016).

In time-domain (TD), the IP phenomenon manifests itself as a transient potential rise/decay following the switch on/off of an electric current induced through a medium. In frequency-domain (FD), this corresponds to a phase shift between the applied current and the arising potential. The IP effect of a material can thus be described by a frequency-dependent complex electrical resistivity. However, no universal physical model is available to describe the effect, why IP often is parameterized using phenomenological models.

The classic Debye model describes the simplest form of a dielectric relaxation response to an alternating current. Cole and Cole (1941) extended the Debye model to account for new experimental observations on different materials. The original Cole-Cole model, expressed in terms of a complex dielectric constant, was later rewritten by Pelton

EAGE Publications B.V., PO Box 59, 3990 DB, Houten, The Netherlands

et al. (1978) to describe the complex resistivity response of mineralized rocks. A complex conductivity form of the original Cole-Cole model is often encountered in literature as well (e.g. Tarasov and Titov, 2013).

Today, the Cole-Cole model (in resistivity or conductivity form) is one of the most prevailing models used for parameterization and inversion of TD IP data (e.g. Yuval and Oldenburg, 1997, Hönig and Tezkan, 2007, Fiandaca et al., 2012) as well as FD IP data (e.g. Yoshioka and Zhdanov, 2005, Loke et al., 2006).

Madsen et al. (2017) presented a sensitivity analysis of Cole-Cole parameters retrieved from TD IP data. In this study, the Cole-Cole model (resistivity form) was used in terms of the following parameters: the direct current resistivity (ρ_0), the intrinsic chargeability (m_0) as described by Seigel (1959), the relaxation time (τ_ρ) and the frequency exponent (C). Here, the τ_ρ symbol is used instead of the classic τ symbol for stressing the fact that τ_ρ refers to the resistivity Cole-Cole model.

The sensitivity analysis proved that spectral Cole-Cole parameters can be retrieved from TD IP data when using full-decay data and an acquisition range above 2.5 decades in time, but that the resolution of the Cole-Cole parameters decreases significantly for small values of C and for values of τ_ρ far outside the acquisition range (Madsen et al., 2017). Furthermore, a strong correlation between m_0 and C was detected in both synthetic generated data and field data. The correlation between m_0 and C have also been detected from inversion of FD IP data (Bérubé et al., 2017).

To improve the model resolution retrieved from inversion of IP data, we suggest three re-parametrizations of the Cole-Cole model: The Maximum Phase Angle (MPA) Cole-Cole, the Maximum Imaginary Conductivity (MIC) Cole-Cole model and the Minimum

EAGE Publications B.V., PO Box 59, 3990 DB, Houten, The Netherlands

Imaginary Resistivity (MIR) Cole-Cole model. The sensitivity of the classic and the new Cole-Cole model parameters are compared using Markov Chain Monte Carlo (MCMC) inversion, which allows us to study the posterior probability distributions of each parameter and quantify uncertainties without linearization. We show that models, which are poorly resolved from inversion with the classic Cole-Cole model (e.g. due to low signal-to-noise ratio) can be resolved well with the new re-parameterizations and that the re-parameterizations work equally well for TD and FDIP data. In addition, we present a field example that shows that gradient-based inversions benefits from the re-parameterizations as well and consequently obtain a significantly deeper depth of investigation.

RE-PARAMETRIZATIONS OF COLE-COLE

The Cole-Cole model describing the complex resistivity is defined as (Pelton et al., 1978)

$$\tilde{\rho}(\omega) = \rho'(\omega) + i\rho''(\omega) = \rho_0\left[1 - m_0\left(1 - \frac{1}{1+(i\omega\tau_\rho)^C}\right)\right], \quad (1)$$

where ρ_0, m_0, τ_ρ, and C are the previously described Cole-Cole parameters, $\omega = 2\pi f$ is the angular frequency, and i is the imaginary unit. The model space is thus defined as

$$\boldsymbol{m}_{\boldsymbol{resistivity\ Cole-Cole}} = \{\rho_0, m_0, \tau_\rho, C\}. \quad (2)$$

Alternatively, the Cole-Cole model can also be presented in its conductivity form (e.g. Tarasov and Titov, 2013),

EAGE Publications B.V., PO Box 59, 3990 DB, Houten, The Netherlands

$$\tilde{\sigma}(\omega) = \sigma'(\omega) + i\sigma''(\omega) = \sigma_0 \left[1 - \frac{m_0}{1-m_0}\left(1 - \frac{1}{1+(i\omega\tau_\sigma)^C}\right)\right], \quad (3)$$

with the corresponding model space defined as

$$\boldsymbol{m}_{\textbf{conductivity Cole–Cole}} = \{\sigma_0, m_0, \tau_\sigma, C\}. \quad (4)$$

The conductivity and resistivity Cole-Cole models (CCC and RCC) are identical, i.e. $\tilde{\sigma}(\omega) = 1/\tilde{\rho}(\omega)$, when the respective relaxation times τ_σ and τ_ρ obey the following relation:

$$\tau_\sigma = \tau_\rho \cdot (1 - m_0)^{1/C}. \quad (5)$$

The inverse of τ_σ represents the angular frequency of the maximum of the imaginary conductivity,

$$\sigma''_{max} = \sigma''(\omega = 1/\tau_\sigma), \quad (6)$$

while the inverse of τ_ρ represents the angular frequency of the minimum of the imaginary resistivity,

$$\rho''_{min} = \rho''(\omega = 1/\tau_\rho). \quad (7)$$

Fig. 1 shows the absolute value of the complex resistivity $|\tilde{\rho}|$, the phase of the complex conductivity φ, the imaginary conductivity σ'' and the imaginary resistivity ρ'' of the Cole-Cole model as a function of frequency for the model defined by $\rho_0 = 100\ \Omega m$, $m_0 = 500\ mV/V$, $\tau_\rho = 0.1\ s$ and $C = 0.2$. The high m_0-value was chosen to emphasize the frequency variation of the spectrum.

The phase of the complex conductivity, $\varphi(\omega)$ (Fig. 1b), can be defined both in terms of equation 1 and equation 3, so

EAGE Publications B.V., PO Box 59, 3990 DB, Houten, The Netherlands

$$\varphi(\omega) = tan^{-1}\left(\frac{\sigma''(\omega)}{\sigma'(\omega)}\right) = -tan^{-1}\left(\frac{\rho''(\omega)}{\rho'(\omega)}\right). \quad (8)$$

The phase reaches a maximum, φ_{max}, at an angular frequency $\omega_\varphi = 1/\tau_\varphi$ (Fig 1b),

$$\varphi_{max} = tan^{-1}\left(\frac{\sigma''\left(1/\tau_\varphi\right)}{\sigma'\left(1/\tau_\varphi\right)}\right) = -tan^{-1}\left(\frac{\rho''\left(1/\tau_\varphi\right)}{\rho'\left(1/\tau_\varphi\right)}\right), \quad (9)$$

where the relaxation time, τ_φ, is linked to τ_ρ and τ_σ through the other Cole-Cole parameters m_0 and C:

$$\tau_\varphi = \tau_\rho \cdot (1 - m_0)^{1/2C} = \tau_\sigma \cdot (1 - m_0)^{-1/2C}. \quad (10)$$

The differences between τ_ρ, τ_σ and τ_φ increase with an increase of m_0 and/or with a decrease of C. Furthermore, φ_{max}, as well as σ''_{max} and ρ''_{min}, increases with m_0 and C. The dependence of the phase shift on both m_0 and C is the main reason for the parameter correlations described by Madsen et al. (2017) and Bérubé et al. (2017), as depicted in Fig. 2. In fact, with frequency ranges below 4 decades, which is typical in field IP surveying, similar variations in the phase spectrum can be induced by decreasing m_0 (magenta line, Fig. 2a) or C (blue line, Fig. 2a). A similar equivalence is found in TD, with acquisition ranges below 4 decades (Fig. 2b). However, it has to be noted that in order to take the acquisition range in the TD forward response into account, the current waveform, and in particular the duration of the current injection, has to be modelled. This explains the difference between the step response (dashed black line) and the response with limited acquisition range (continuous black line) in Fig. 2b.

EAGE Publications B.V., PO Box 59, 3990 DB, Houten, The Netherlands

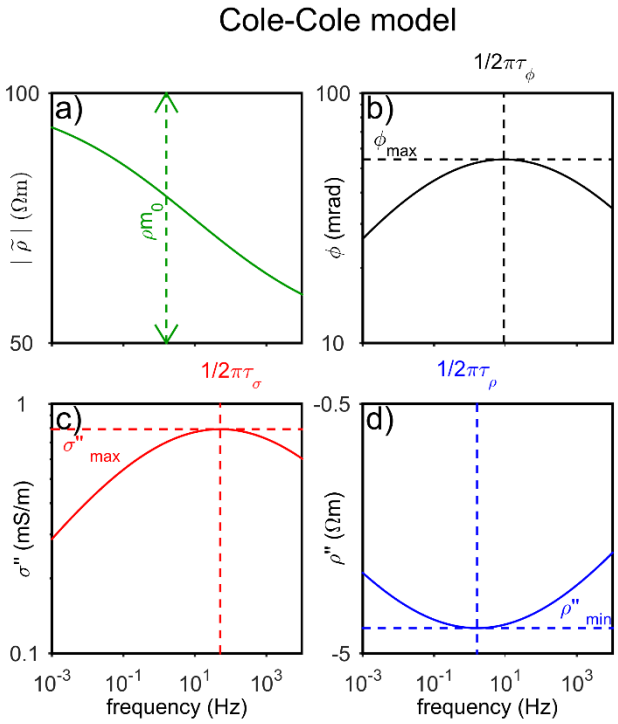

Figure 1. *Cole-Cole model defined by* $\rho_0 = 100\,\Omega m$, $m_0 = 500\,mV/V$, $\tau_\rho = 0.1\,s$, *and* $C = 0.2$. *a) amplitude of the complex resistivity; b) phase of the complex conductivity; c) imaginary conductivity; d) imaginary resistivity.*

EAGE Publications B.V., PO Box 59, 3990 DB, Houten, The Netherlands

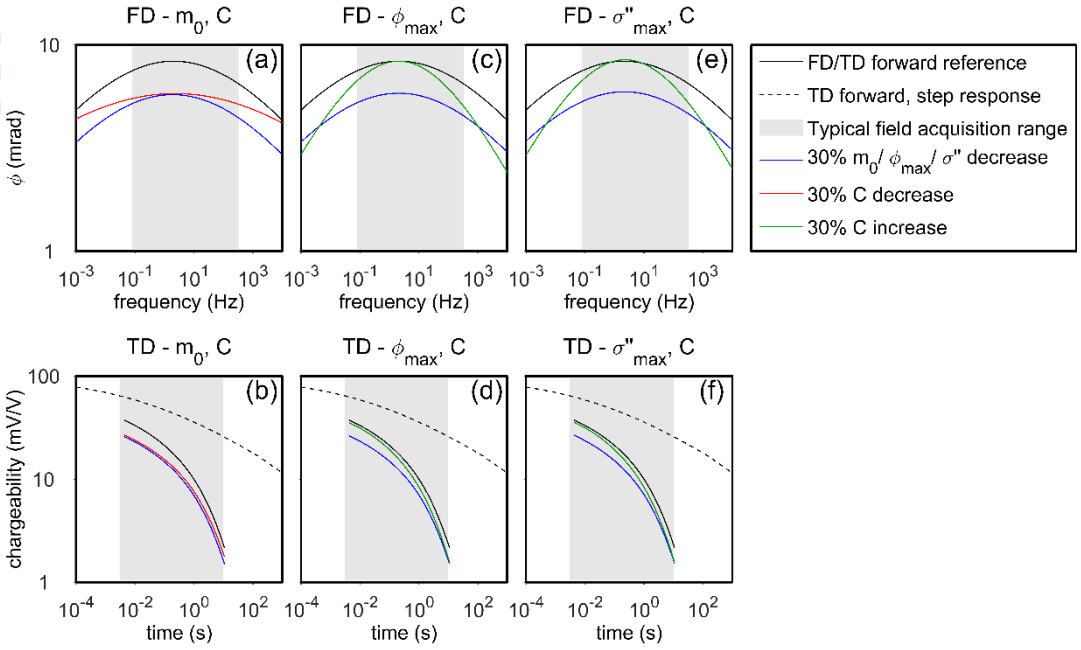

Figure 2. *Variations of frequency-domain (FD) and time-domain (TD) responses with* $m_0, \varphi_{max}, \sigma''_{max}$ *and* C*. Reference model:* $\rho_0 = 100\ \Omega m$, $m_0 = 100\ mV/V$, $\tau_\rho = 0.1\ s$, *and* $C = 0.2$. *a) FD responses,* m_0 *and* C *variations; b) TD responses,* m_0 *and* C *variations; c) FD responses,* φ_{max} *and* C *variations; d) TD responses,* φ_{max} *and* C *variations; e) FD responses,* σ''_{max} *and* C *variations; f) TD responses,* σ''_{max} *and* C *variations.*

Maximum Phase Angle (MPA)

We suggest a re-parameterization of the Cole-Cole model where instead of m_0 and τ_ρ the maximum phase $\varphi_{\max}$ (equation 9 and Fig. 1b) and the phase relaxation time τ_φ (equation 10 and Fig. 1b) are used as model parameters. The re-parameterized model space becomes:

$$\boldsymbol{m}_{\boldsymbol{MPA\ Cole-Cole}} = \{\rho_0, \varphi_{\max}, \tau_\varphi, C\}. \quad (11)$$

EAGE Publications B.V., PO Box 59, 3990 DB, Houten, The Netherlands

In Fig. 2c the variations in the phase spectrum induced by a decrease of $\varphi_{\max}$ (blue line) and an increase of C (green line) are shown. In comparison to the classic Cole-Cole parameterization (Fig. 2a), a much bigger data difference is present between the responses, meaning that $\varphi_{\max}$ and C are less correlated than m_0 and C. The same applies in the comparison of the TD responses in Fig. 2b and Fig. 2d. In TD, we see that the green response (C 30% decrease) follows the reference model at the early time and the blue response ($\varphi_{\max}$ 30% decrease) at the late times (Fig. 2d).

To summarize, the parameter $\varphi_{\max}$ controls the FD maximum phase shift, as well as the magnitude of the TD decays, while the parameter C controls the width of the phase shift and the decay shape.

Given the MPA Cole-Cole model parameters $\{\rho_0, \varphi_{\max}, \tau_\varphi, C\}$, the corresponding parameters of the RCC (or CCC) model $\{\rho_0, m_0, \tau_\rho, C\}$ can be easily computed through an iterative approach (See Appendix A).

Maximum Imaginary Conductivity (MIC)

Another re-parameterization of the classic Cole-Cole model is the Maximum Imaginary Conductivity (MIC) Cole-Cole model. The MIC model space is defined in terms of

$$\boldsymbol{m}_{\boldsymbol{MIC\ Cole-Cole}} = \{\sigma_0, \sigma''_{max}, \tau_\sigma, C\}, \quad (12)$$

where σ''_{max} is the maximum of the imaginary conductivity (Fig. 1c) as defined as in equation 6.

The influence of changes in σ''_{max} and C on the phase shift and the chargeability is shown in Fig. 2e and Fig. 2f, respectively. The responses are very similar to those of $\varphi_{\max}$, because $\sigma''_{max} \cong \sigma_0 \varphi_{\max}$. Given the MIC Cole-Cole model parameters, the

EAGE Publications B.V., PO Box 59, 3990 DB, Houten, The Netherlands

corresponding parameters of the CCC models can be computed directly as shown in Appendix A.

Minimum Imaginary Resistivity (MIR)

The resistivity equivalence to the MIC Cole-Cole model is the Minimum Imaginary Resistivity (MIR) Cole-Cole model. The model space is defined in terms of

$$\boldsymbol{m}_{\boldsymbol{MIR\ Cole-Cole}} = \{\rho_0, \rho''_{min}, \tau_\rho, C\}, \quad (13)$$

where ρ''_{min} is the minimum of the imaginary resistivity (Fig. 1d) as defined in equation 7. The responses of the MIR Cole-Cole model are not shown in Fig. 2 as they are similar to those of $\varphi_{\max}$ and σ''_{max}, because $\rho''_{min} \cong -\rho_0 \varphi_{\max}$.

Given the MIR Cole-Cole model parameters, the corresponding parameters of the RCC model can be computed directly as shown in Appendix A.

DATA SPACE

Time-domain data

The data space, d_{obs}, for the MCMC and gradient-based inversions of TD IP data consists of apparent resistivity and full-decay chargeability values:

$$\boldsymbol{d}_{\boldsymbol{obs}} = \{\rho_a, M_i\}, i = 1{:}\, N_{gates} \quad (14)$$

where ρ_a (Ωm) is the apparent resistivity and the data-space chargeability, M_i (mV/V), is computed in each time-gate, i, of the transient full-decay IP signal as described by

EAGE Publications B.V., PO Box 59, 3990 DB, Houten, The Netherlands

Olsson et al. (2015). If no negative data are present, the inversion can be performed in logarithmic data space.

A waveform with a 100% duty cycle, where the TD IP data are measured in the current-on time as described by Olsson et al. (2015), is applied for both generation of synthetic data and in the field data acquisition. For the synthetic data, each IP signal is recorded from 2.6 ms to 12,000 ms and the decay is divided into 26 time-gates (listed in Appendix B) with an approximately log-increasing gate width to improve the signal-to-noise ratio at late times (Fiandaca et al., 2012). The same acquisition range (about 3.5 decades) is also obtainable in field surveying when full-waveform recordings are processed for harmonic de-noising and background removal (see details in the field example). Three stacks have been model in the synthetic forward responses, while two stacks have been used in the field example. The used quadrupoles and the noise model are described in the separate results section for the synthetic data and field data.

Frequency-domain data

For the FD IP data, the data space consists of the amplitude, A_j (Ωm), and the data-space phase, φ_j (mrad), which are measured at a range of frequencies, j. Similarly to the phase defined in model space, the data space phase is defined here as the phase of the complex conductivity. The data vector applied in the inversion becomes:

$$\boldsymbol{d_{obs}} = \{\varphi_j, A_j\}, j = 1{:}\, N_{frequencies} \quad (15)$$

For the synthetic data, we simulate measurements at 13 frequencies in the range from 0.08 Hz to 327 Hz and thereby get 26 data values in total, the same as the number of time-gates applied in TD. In total, about 3.5 decades in frequency are spanned by the data, with first and last frequency approximately equal to the inverse of the last and first

EAGE Publications B.V., PO Box 59, 3990 DB, Houten, The Netherlands

TD center gate time, respectively. The applied frequencies are listed in Appendix B. Used quadrupoles and noise model are described in the result section.

INVERSION METHODOLOGY

The 1D TD forward response of synthetic data is computed using the algorithm presented in Fiandaca et al. (2012). This algorithm computes the full-decay IP response and models the transmitter current waveform and the receiver transfer function accurately. The same algorithm has been applied to compute the FD forward response by disregarding the time-domain transform. An extension of the algorithm, which computes the 2D forward response (Fiandaca et al., 2013), has been applied in the inversion of field data.

In the following analyses of the re-parameterizations of the Cole-Cole model, we have used two different inversion methods. First, a MCMC inversion algorithm is used to compute a non-linearized uncertainty analysis of all the model parameters. Hereafter, a field example is inverted in 2D using a gradient-based inversion approach in order to show how field surveys may benefit from the re-parameterizations.

MCMC inversion

With the MCMC inversion method, it is possible to investigate the distribution of models that fit a given data set. Compared to a gradient-based inversion, the MCMC method (as well as other statistical inversion approaches) has an advantage when it comes to quantifying parameter uncertainties and correlations without linearizing the problem as described by Chen et al. (2008) and Madsen et al. (2017).

EAGE Publications B.V., PO Box 59, 3990 DB, Houten, The Netherlands

In this study, we apply a Metropolis-Hastings sampling algorithm (Metropolis et al., 1953, Hastings, 1970) that, based on a random-walk in the model space, samples models according to their likelihood. The sampled models make up a Markov Chain, which converges toward the posterior probability distribution of the model space.

The applied sampling algorithm, which is described in details in Madsen et al. (2017), works in two steps. First, a model is proposed. Next, the model is accepted to the Markov Chain with an acceptance probability that depends only on the last accepted model in the chain and none of the previous models. These two steps are repeated a predefined number of times or until the distribution of the sampled models (the posterior probability distribution) has converged.

Because we apply a symmetric model proposer, where the possibility of walking from model $\boldsymbol{m_i}$ to $\boldsymbol{m_j}$ is the same as walking from $\boldsymbol{m_j}$ to $\boldsymbol{m_i}$, the acceptance probability of $\boldsymbol{m_i}$ can be computed simply as a likelihood ratio (Malinverno, 2002):

$$P_{acc}(\boldsymbol{m_i}) = min\left[1, \frac{P_{like}(\boldsymbol{m_i})}{P_{like}(\boldsymbol{m_{i-1}})}\right], \tag{16}$$

where the likelihood function is given as by Mosegaard and Tarantola (2002):

$$P_{like}(\boldsymbol{m}) = k \cdot \exp\left[\frac{1}{2}(g(\boldsymbol{m}) - \boldsymbol{d_{obs}})^T \boldsymbol{C_{obs}}(g(\boldsymbol{m}) - \boldsymbol{d_{obs}})\right], \tag{17}$$

where $g(\boldsymbol{m})$ is the forward response of the model $\boldsymbol{m}$, $\boldsymbol{C_{obs}}$ is the covariance matrix of the observed data, $\boldsymbol{d_{obs}}$, and k is a normalization constant.

Due to the logarithmic transform applied on the model parameters, uncertainties are given as standard deviation factors (STDFs), where the STDF of the marginal posterior probability distribution, PDF (defined in the logarithmic space), can be computed as

EAGE Publications B.V., PO Box 59, 3990 DB, Houten, The Netherlands

$$STDF = exp(STD(PDF)). \quad (18)$$

Assuming the model parameters to be normally distributed in the logarithmic space, the ±STD limits are given by

$$\frac{\mu}{STDF} < \mu < \mu \cdot STDF, \quad (19)$$

were μ is the mean of the distribution. So, with $STDF$ = 1.1 the model parameter has a relative uncertainty of 10%, while with $STDF$ = 2.0 the uncertainty grows 10-fold to 100%. Using the terminology of Auken et al. (2005), a STDF < 1.2 is a well-resolved parameter, 1.2 < STDF < 1.5 is a moderately resolved parameter, 1.5 < STDF < 2 is a poorly resolved parameter and a STDF > 2 is an unresolved parameter.

The posterior distribution of the classic Cole-Cole parameters is related to the ones of the re-parameterizations. In theory, with a complete knowledge of the posterior distribution of the Cole-Cole model (included the asymptotic behavior) and an analytical expression for the mapping between the parameterizations, it would be possible to obtain the posterior distribution of the re-parameterization from the one of the classic Cole-Cole. This is difficult to obtain in practice, why we have chosen to sample the distributions for each parameterization individually.

Gradient-based inversion

For inversion of field data, we apply the gradient-based 2D inversion scheme that is described in detail by Fiandaca et al. (2013). The algorithm applies the first term Taylor expansion for linearization and uses a iterative method to minimizes the misfit,

$$\chi = \left(\frac{\delta \boldsymbol{d}^T \boldsymbol{C}_{obs}^{-1} \delta \boldsymbol{d} + \delta \boldsymbol{r}^T \boldsymbol{C}_R^{-1} \delta \boldsymbol{r}}{N_d + N_R} \right)^{\frac{1}{2}}, \quad (20)$$

EAGE Publications B.V., PO Box 59, 3990 DB, Houten, The Netherlands

where $\delta \boldsymbol{d}$ is the data misfit, $\boldsymbol{C}_{obs}$ is the covariance matrix of the observed data, $\delta \boldsymbol{r}$ is the model roughness and $\boldsymbol{C}_R$ is the covariance on the roughness constraints. N_d and N_R are the numbers of data parameters and roughness constrains, respectively. No priors have been used in the inversion, however, if priors were applied this would add an extra term to equation 20.

From the inversion result, a linearized uncertainty analysis is computed based on the posterior covariance matrix (Tarantola and Valette, 1982),

$$\boldsymbol{C}_{est} = \left(\boldsymbol{G}^T {\boldsymbol{C}_{obs}}^{-1} \boldsymbol{G} + \boldsymbol{R}^T {\boldsymbol{C}_R}^{-1} \boldsymbol{R}\right)^{-1}, \quad (21)$$

where $\boldsymbol{G}$ is the Jacobian matrix holding the partial derivatives of the mapping and $\boldsymbol{R}$ is the roughness matrix. Equivalent to the uncertainty analysis in the MCMC approach (equation 18 and equation 19), a STDF of the $i'th$ model parameter m_i can then be computed as

$$STDF(m_i) = \exp\left(\sqrt{C_{est(i,i)}}\right). \quad (22)$$

The STDFs computed for the gradient-based inversion (using equation 21 and equation 22) are influenced by the values of the roughness constrains, why they should only be seen as a relative measure of the uncertainty and cannot be directly compared to the STDFs of constraint-free inversions (either MCMC or other gradient-based results).

Alongside the linearized uncertainty analysis in terms of STDFs, the depth of investigation (DOI) of the inversion model is computed. The DOI algorithm used in this study is based on a cumulated approximated analysis (CAA) that incorporates the actual output model from the inversion as well as the data errors, as described in Fiandaca et al. (2015). For a given depth D, the CAA computes the data-driven (i.e. $\boldsymbol{C}_R = 0$ in

EAGE Publications B.V., PO Box 59, 3990 DB, Houten, The Netherlands

equation 21) cumulated uncertainty analysis, model column by model column. This is done by cumulating the sensitivity of all the model cells below the depth D. A threshold value for the STDF of the CAA is defined, and the DOI is computed as the depth at which this threshold is reached. Based on experience, DOI threshold values between 2 and 5 gives reasonable DOI estimations. The values of the DOI threshold are usually increased for the τ parameter, which is significantly less resolved and for which the order of magnitude is of interest even when the parameter resolution is low. In this study, the DOI threshold is STDF = 4 for all parameter except τ, for which STDF = 20. The approximation in the CAA algorithm consists in neglecting the correlations between model parameters belonging to different model columns (lateral data correlation), but still considering the correlation among the Cole-Cole parameters for each model column. This means that the DOI algorithm gives results that depends on the actual model parameterization used in the inversion, and can thus be used as a comparative factor between the parameters of the different Cole-Cole parameterizations.

UNCERTAINTY ANALYSIS

In the following, we presents the results of an uncertainty analysis computed using MCMC methods. The MCMC inversion results are presented as marginal posterior probability distributions, which are the distributions of the sampled models shown for each individual model parameter, and the uncertainty is given as the STDF of each distribution as defined in equation 18.

EAGE Publications B.V., PO Box 59, 3990 DB, Houten, The Netherlands

The applied noise model has a relative and an absolute term, for both TD and FD data. In TD, a 2% standard deviation has been applied to the resistivity data; 10% relative standard deviation plus 0.2 mV/V absolute noise has been applied on the IP data. Similarly, in FD a 2% standard deviation is considered for the amplitude data; 10% relative standard deviation plus 0.2 mrad absolute noise has been applied on the phase data.

A homogenous half space example

Synthetic data have been generated from a homogenous half-space model using one quadrupole with electrode spacing $|AB| = 7.5$ m and $|MN| = 2.5$ m.

Five different parameterizations have been investigated: the classic Cole-Cole model in both conductivity form (CCC) and resistivity form (RCC); the three new re-parameterizations (MPA, MIC, MIR). The values of the parameters for all parameterizations were derived from the CCC model: $\sigma_0 = 10\, mS/m$, $m_0 = 100\, mV/V$, $\tau_\sigma = 0.1\, s$, and $C = 0.2$. MCMC inversions of TD and FD synthetic data were performed for each parameterization individually using five MCMC runs with different starting models and with one million model proposes (iterations) in each run.

For both TD and FD, the inversion results from the CCC model and the MIC Cole-Cole model are presented in Fig. 3. The posterior probability distributions are plotted together with the true model (red line) and the STDFs.

For both TD and FD, the resolution of σ_0, τ_σ and C are the same independent on the parameterization (Fig. 3). However, the resolution of σ''_{max} is significantly better than the resolution of m_0. As given by the STDFs, it is approximately a 3-fold improvement in both TD (from STDF = 1.4 to STDF = 1.12) and FD (from STDF = 1.13 to STDF =

EAGE Publications B.V., PO Box 59, 3990 DB, Houten, The Netherlands

1.04). The results of the MPA and the MIR model are very similar to those of the MIC, why they are not show here, however, the STDF are listed in Table 1. Overall, the results show that the FD data gives a better resolved than the TD data. This it is due to the choice of the relaxation time ($\tau_\sigma = 0.1$). If we instead set $\tau_\sigma = 1$, the TD data give the best resolution (see discussion).

Fig. 4 shows the cross-plots of m_0 and σ''_{max} with the remaining Cole-Cole parameters. A non-linear correlation is present between m_0 and τ_σ (Fig. 4b), while the correlation between σ''_{max} and τ_σ is linear and spans a smaller area of the model space (Fig. 4e). The correlation between C and m_0 or σ''_{max} are both non-linear, but we see that σ''_{max} spans a smaller parameter range. Consequently, σ''_{max} is resolved better than m_0.

EAGE Publications B.V., PO Box 59, 3990 DB, Houten, The Netherlands

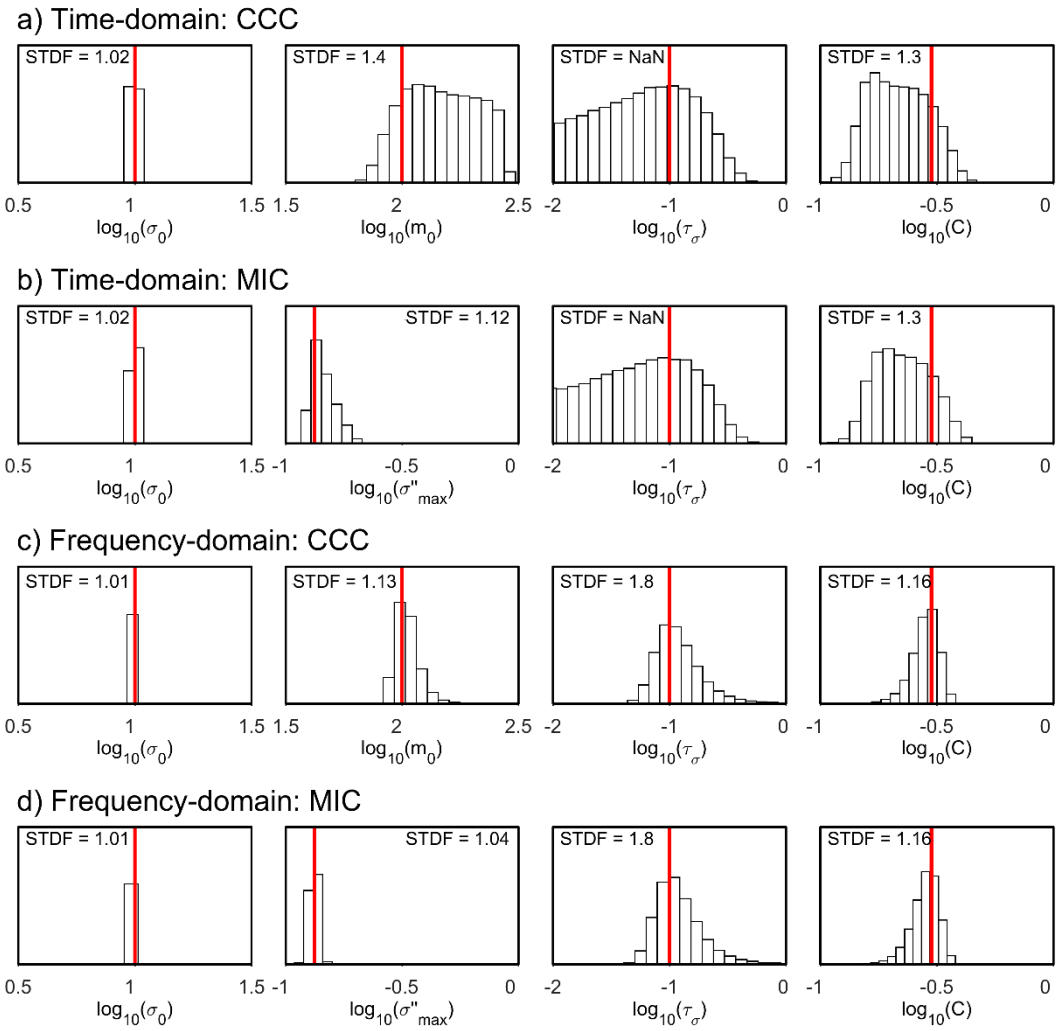

Figure 3. *Posterior probability distributions of a homogenous half space model with the parameters:* $\sigma_0 = 10\ mS/m$, $m_0 = 100\ mV/V$ ($\sigma''_{max} = 0.13\ mS/m$), $\tau_\sigma = 0.1$ *s and* $C = 0.3$. *The distributions are shown for: a) time-domain, conductivity Cole-Cole; b) time-domain, MIC Cole-Cole; c) Frequency-domain, conductivity Cole-Cole; d) frequency-domain, MIC Cole-Cole. The red line marks the true model. NaN indicates that the distribution have not converged. Note that the distributions of* τ_σ *are wider scaled.*

EAGE Publications B.V., PO Box 59, 3990 DB, Houten, The Netherlands

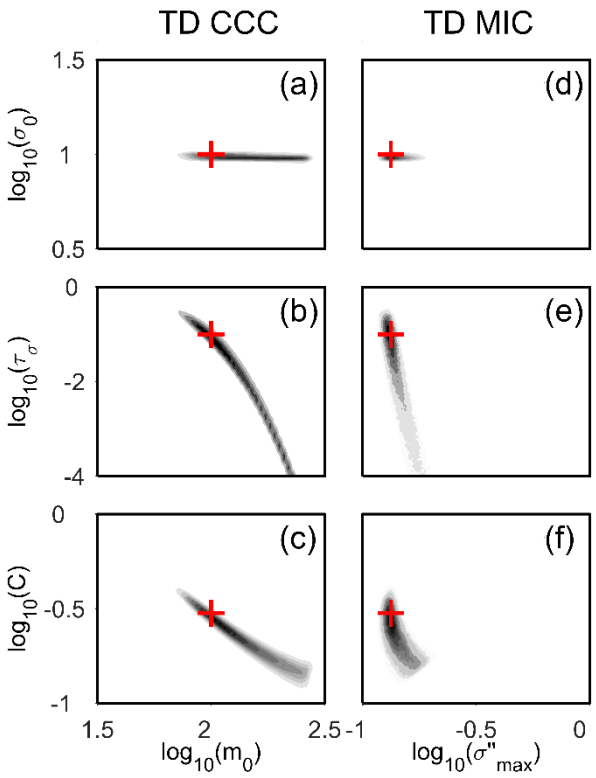

Figure 4. *Cross-plots of the model parameters determined from inversion of time-domain data representing a homogenous half space:* $\sigma_0 = 10\ mS/m$ $m_0 = 100\ mV/V$ $(\sigma''_{max} = 0.13\ mS/m)$, $\tau_\sigma = 0.1\ s$ *and* $C = 0.3$. *Two different models have been used for parameterization of IP: abc) the conductivity Cole-Cole model; def) the MIC Cole-Cole model. The red cross marks the true model.*

Changing the frequency exponent

To study the influence of the re-parameterization on models with different resolutions, the values of C have been varied between $C = 0.2$ and $C = 0.6$ in the CCC model, while the remaining parameters have been kept constant (i.e. $\sigma_0 = 10\ mS/m$, $m_0 = 100\ mV/V$, and $\tau_\sigma = 0.1\ s$). Variation in C in the CCC model gives rise to changes in not just C, but also in σ''_{max}, φ_{max}, ρ''_{min}, τ_φ and τ_ρ in the equivalent re-parameterized models, as these parameters are functions of C and m_0.

EAGE Publications B.V., PO Box 59, 3990 DB, Houten, The Netherlands

As the STDFs of σ_0, ρ_0, τ_φ, τ_σ, τ_ρ and C do not vary significantly between parameterizations (as seen in Fig. 3) and the CCC and RCC results are equivalent, only the STDFs of m_0, φ_{max}, σ''_{max} and ρ''_{min} are presented in the uncertainty analysis in Table 1.

For TD and FD data, the resolution of m_0, φ_{max}, σ''_{max} and ρ''_{min} decreases as the value of C is decreased. For $C = 0.2$, the resolution of φ_{max}, σ''_{max} and ρ''_{min} is close to a 10-fold improvement compared to the resolution of m_0. For $C = 0.4$, the improvement is down to a 2-fold in TD. When $C = 0.6$ the uncertainty is approximately the same for all the parameterizations. This shows that especially poorly resolved models benefit form the re-parameterizations, but the impact on well resolved models is minor.

Table 1: *Uncertainty analysis for different parameterizations for different values of C. Using MCMC inversion, five different models have been analyzed where the value of C has been varied between 0.2 and 0.6 and the remaining parameters have been kept constant: $\sigma_0 = 10\ mS/m$, $m_0 = 100\ mV/V$, and $\tau_\sigma = 0.1\ s$. The results are shown from the conductivity Cole-Cole ($\boldsymbol{m_0}$), the MIC Cole-Cole ($\boldsymbol{\sigma''_{max}}$), the MIR Cole-Cole ($\boldsymbol{\rho''_{min}}$) and the MPA Cole-Cole ($\boldsymbol{\varphi_{max}}$) parametrization. The uncertainties are given as the STDF of the marginal posterior probability distributions.*

	Time-domain STDFs				**Frequency-domain STDFs**			
C	$\boldsymbol{m_0}$	$\boldsymbol{\sigma''_{max}}$	$\boldsymbol{\rho''_{min}}$	$\boldsymbol{\varphi_{max}}$	$\boldsymbol{m_0}$	$\boldsymbol{\sigma''_{max}}$	$\boldsymbol{\rho''_{min}}$	$\boldsymbol{\varphi_{max}}$
0.2	1.7	1.13	1.12	1.11	1.6	1.06	1.07	1.06
0.3	1.4	1.13	1.12	1.11	1.13	1.04	1.04	1.04
0.4	1.2	1.12	1.10	1.10	1.05	1.04	1.04	1.04
0.5	1.11	1.06	1.06	1.05	1.03	1.04	1.04	1.04
0.6	1.07	1.05	1.05	1.05	1.03	1.04	1.04	1.04

EAGE Publications B.V., PO Box 59, 3990 DB, Houten, The Netherlands

Changing the noise model

In the following, we show the influence of the noise model on the resolution capabilities of the classic Cole-Cole model compared to that of the re-parameterizations. This is done by assuming different noise levels in the data set generated from the previous described model. The noise levels on the FD /TD data-space phase/chargeability values are: 5% relative noise plus 0.1 (mrad for FD and mV/V for TD) absolute noise; 10% relative noise plus 0.2 mrad/mV/V absolute noise (used in the previous examples); 15% relative noise plus 0.3 mrad/mV/V absolute noise.

The results of the uncertainty analysis are presented in Table 2 as the STDFs of the marginal posterior probability distributions of m_0, σ''_{max}, ρ''_{min} and φ_{max}. For all parameterizations, we see that as the noise level is increases, the STDF of the model parameters increases as well. This is also valid for the parameters not shown in the table. The analyses show that the resolution improvements gained from the re-parameterizations, which have been documented in the previous figures, are valid for all the different noise levels. For the low noise level, the improvement is between 3-fold and 4-fold for TD and 2-fold for FD. For the high noise level, the improvement is 2.5-fold in TD and 4-fold in FD. As seen with the example in Fig. 3, the resolution improvement gained with the re-parameterizations is less pronounced for the remaining parameters.

Table 2: *Uncertainty analysis of the influence of three different noise models on the resolution capabilities of the different parameterizations. The model has the parameters:* $\sigma_0 = 10\ mS/m$, $m_0 = 100\ mV/V$, $\tau_\sigma = 0.1\ s$ *and* $C = 0.3$ *The results are shown from the conductivity Cole-Cole* ($\boldsymbol{m_0}$)*, the MIC Cole-Cole* ($\boldsymbol{\sigma''_{max}}$)*, the MIR Cole-Cole* ($\boldsymbol{\rho''_{min}}$) *and the MPA Cole-Cole* ($\boldsymbol{\varphi_{max}}$) *parametrizations. The*

EAGE Publications B.V., PO Box 59, 3990 DB, Houten, The Netherlands

uncertainties are given as the STDF of the marginal posterior probability distributions.

	Time-domain			Frequency-domain		
Noise	**5% 0.1 mV/V**	**10% 0.2 mV/V**	**15% 0.3 mV/V**	**5% 0.1 mrad**	**10% 0.2 mrad**	**15% 0.3 mrad**
$\boldsymbol{STDF(m_0)}$	1.2	1.4	1.5	1.05	1.13	1.4
$\boldsymbol{STDF(\sigma''_{max})}$	1.07	1.13	1.2	1.02	1.04	1.08
$\boldsymbol{STDF(\rho''_{min})}$	1.05	1.12	1.2	1.02	1.04	1.09
$\boldsymbol{STDF(\varphi_{max})}$	1.06	1.11	1.2	1.02	1.04	1.08

A multilayer example

Synthetic TD and FD data generated from a three-layered model have been inverted using the CCC model and the re-parameterizations (MIC, MIR and MPA). The model was given the CCC parameters: $\sigma_0 = [50,\ 50, 50]\ mS/m$, $m_0 = [5, 300, 5]\ mV/V$, $\tau_\sigma = [0.1, 3, 5]\ s$, $C = [0.3, 0.3, 0.3]$ and thickness = [7, 7] m. The data were generated from a vertical sounding with 20 quadrupoles, with electrode spacing |AB| = 7.5 - 500 m and |MN| = 2.5 - 65 m.

The inversion results of the TD and FD data show the same features. Furthermore, the MIC, the MIR and the MPA Cole-Cole models preforms equally well. For these reasons, we only present the TD marginal posterior probability distributions of m_0 (CCC) and σ''_{max} (MIC) in Fig. 5.

The inversion results show a 3- to 6-fold improvement in the resolution from m_0 to σ''_{max} in the top and bottom layers where the chargeability is low. It is an improvement from poorly resolved parameters (Fig. 5a and Fig. 5c) to well-resolved parameters (Fig. 5d and Fig. 5f). For the remaining parameters, the differences between the two

EAGE Publications B.V., PO Box 59, 3990 DB, Houten, The Netherlands

parameterizations are negligible. In the second layer, the MIC Cole-Cole model produces a slightly lower STDF of σ''_{max} relative to m_0 (Fig. 5b and Fig. 5e), and again the differences between the parameterizations are negligible for the remaining parameters.

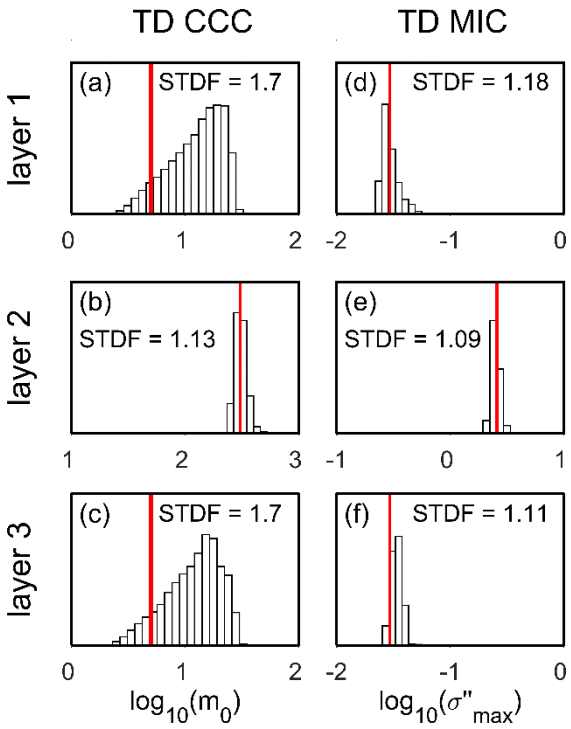

Figure 5. *Marginal posterior probability distribution and STDFs for m_0 (the conductivity Cole-Cole model) and σ''_{max} (the MIC Cole-Cole model) for the three-layer model: $\sigma_0 = [50,\ 50, 50]\ mS/m$, $m_0 = [5, 300, 5]\ mV/V$, $\tau_\sigma = [0.1, 3, 5]\ s$, $C = [0.3, 0.3, 0.3]$ and thickness = [7, 7] m. The red line marks the true model values.*

FIELD EXAMPLE

The field data were acquired at the Samsø island (Denmark). The site geology is very heterogeneous in the top 10-12 m, characterized by late-glacial meltwater deposits and

EAGE Publications B.V., PO Box 59, 3990 DB, Houten, The Netherlands

postglacial freshwater sand and peat. Below that, a clay-till layer approximately 20 m thick is present, followed by a regional aquifer in meltwater sand and gravel deposits. Below the regional aquifer, a till/clay layer is present, approximately at 40 m depth. TD IP data were collected along a 2D profile using 49 electrodes with 3 m spacing, for a total length of 144 m. The quadrupole sequence consisted of a mix of Gradient and Dipole-Dipole arrays, for a total of 1161 quadrupoles. Data were acquired using the ABEM Terrameter-LS instrument (www.guidelinegeo.com), with full-waveform signal sampled at 3750 Hz. The full-waveform signal was processed for harmonic de-noising and background drift removal following (Olsson et al., 2016) and gated using logarithmically-spaced gates from 10^{-3} to 12 s (with ten points per decade). The de-noised and re-gated TDIP data were imported to the Aarhus Workbench software (www.aarhusgeosoftware.dk) for manual processing of the IP decays. Single gates or entire decays showing poor quality, for instance due to poor signal-to-noise ratio, were removed. On average, the TD decays have 3.4 decades of usable time range after processing. A 1% standard deviation has been assigned to the resistivity data; 10% relative standard deviation plus 0.05 mV/V absolute noise has been assigned to the IP data. Vertical and horizontal constraints values, expressed as STDFs, were set up to 1.5 and 1.15, respectively.

Fig. 6 shows the inversion results for the CCC model. Panels a-d represent the uncertainty on the inversion parameters ($\sigma_0, m_0, \tau_\sigma, C$) computed following equation 22, using the final inversion model for the Jacobian computation; panels e-h show the inversion model, for the $\sigma_0, m_0, \tau_\sigma$ and C parameters. Panel i shows the data misfit. On top of the a-d and e-h panels, the DOI is shown as a black line. Fig. 7 shows the results of the MIC inversion, with uncertainty on panels a-b and model on panels e-h for the

EAGE Publications B.V., PO Box 59, 3990 DB, Houten, The Netherlands

inversion parameters $\sigma_0, \sigma''_{max}, \tau_\sigma$ and C, and misfit on panel i. On both Fig. 6 and Fig. 7 the lithological information available from a nearby borehole is superimposed on the inversion.

The σ_0, τ_σ and C inversion results are really similar in the CCC and MIC inversion of Fig. 6 and Fig. 7, both in terms of inversion model (panels e-h), uncertainty (panels a-d) and DOI. Significant differences exist between the m_0 and σ''_{max} results. The uncertainty values decrease with depth much quicker, indicating less resolution at depth. This is reflected also in the DOI estimation that is more than double for the σ''_{max} parameter. Furthermore, a better correlation between geology and σ''_{max} exists, when compared to the m_0 results. The sand layer at 4.0 m depth is better represented in the σ''_{max} section (with values below ~0.05 mS/m), with a superior thickness resolution when compared to the low-m_0 anomaly (with values below ~30 mV/V). Anomalies with high σ''_{max} values (above ~0.15 mS/m) and high m_0 values (above ~70 mV/V) correspond to the till layer (16 m thick) below 8.3 m, but the σ''_{max} anomaly resembles better the geological layer. Finally, the increase in σ''_{max} at depth correlates with the depth of the till/clay layer present below the regional aquifer, at depth of approximately 40 m.

EAGE Publications B.V., PO Box 59, 3990 DB, Houten, The Netherlands

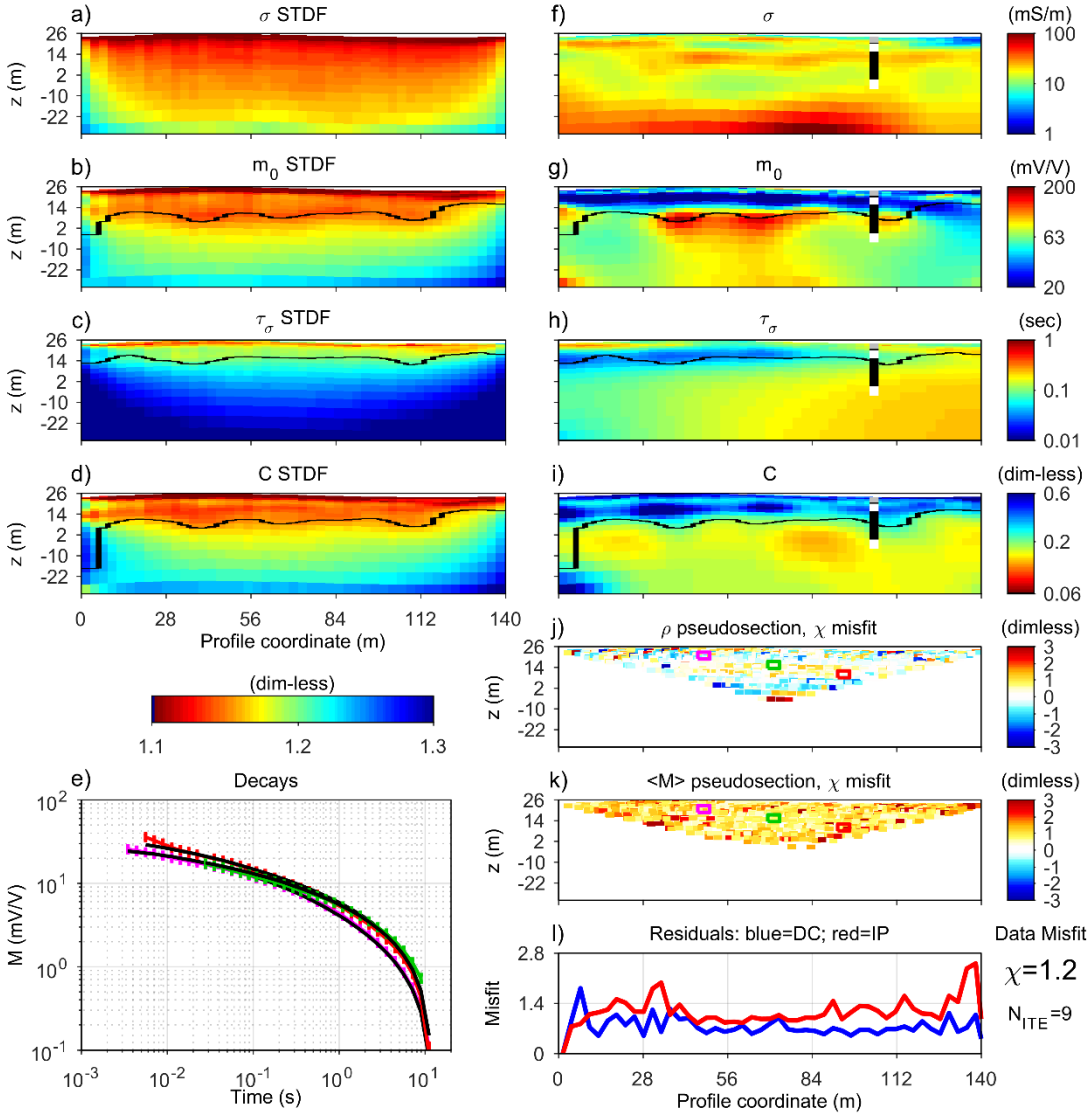

Figure 6. *Inversion model, uncertainty analysis and misfit of field data from Samsø, Denmark, obtained using the conductivity Cole-Cole parameterization. a-d) the uncertainty analysis given as the STDF of the four model parameters; e) three examples of IP decays with error bars (the locations of the data cells are marked in panel j and k) and fitting forward response (black lines); f -i) inversion model with borehole information (white is sand, black is till and grey is silt); j) resistivity pseudosection showing the misfit χ; k) pseudosection of the root mean square χ for the entire IP decay (defined positive). l) misfit of DC (blue) and IP (red) data of the inversion averaged vertically (and over all gates for the IP misfit) along the*

EAGE Publications B.V., PO Box 59, 3990 DB, Houten, The Netherlands

pseudosection. N_{ITE} is the number of iterations. The black lines in panel a-d and f-i are the DOI.

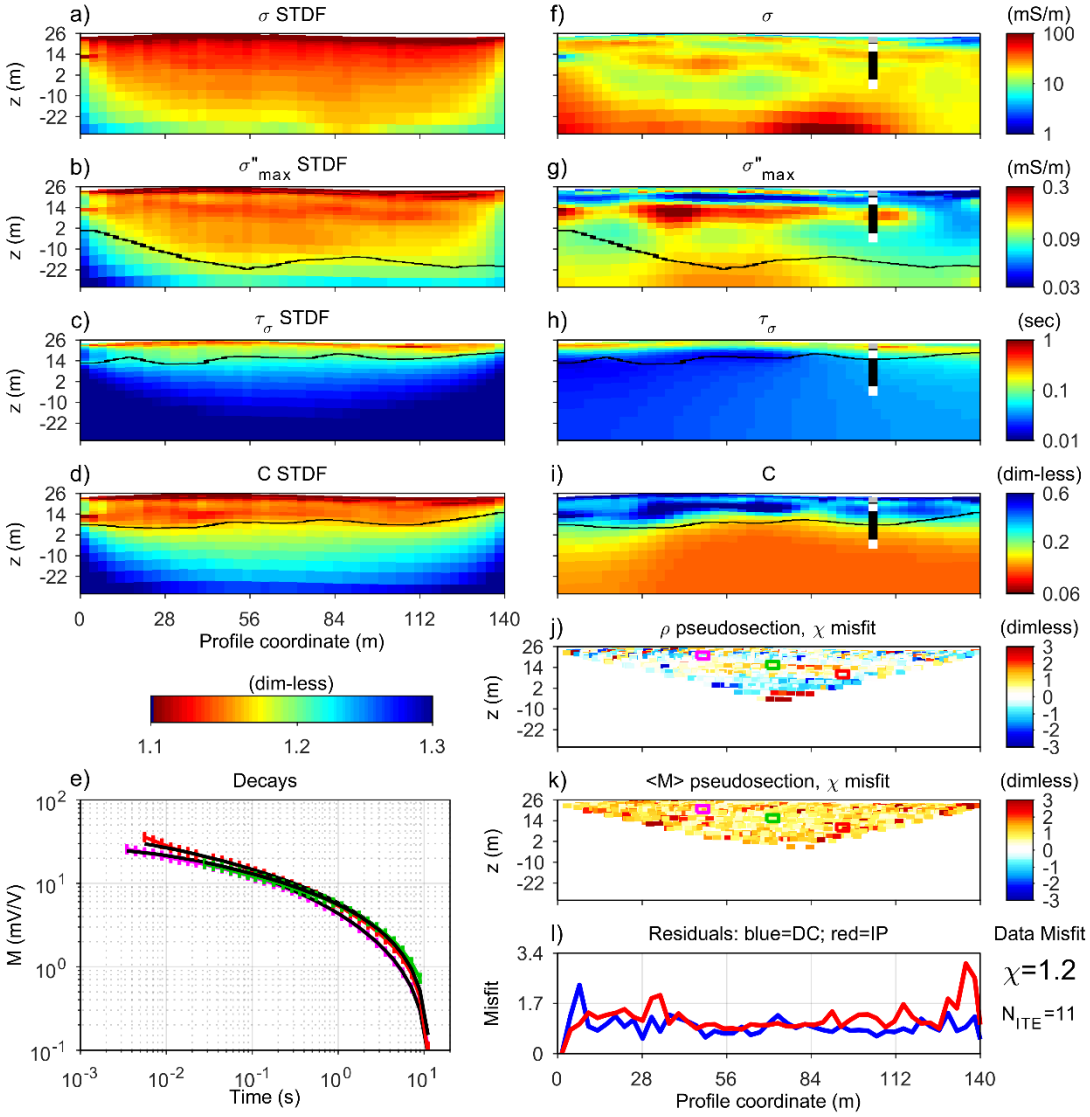

Figure 7: *Inversion model, uncertainty analysis and misfit of field data from Samsø, Denmark, obtained using the MIC Cole-Cole model for parameterization of IP. a-d) the uncertainty analysis given as the STDF of the four model parameters; e) three examples of IP decays with error bars (the locations of the data cells are marked in panel j and k) and fitting forward response (black lines); f -i) inversion model with borehole information (white is sand, black is till and grey is silt); j) resistivity*

EAGE Publications B.V., PO Box 59, 3990 DB, Houten, The Netherlands

pseudosection showing the misfit χ; k) pseudosection of the root mean square χ for the entire IP decay (defined positive). l) misfit of DC (blue) and IP (red) data of the inversion averaged vertically (and over all gates for the IP misfit) along the pseudosection. N_{ITE} is the number of iterations. The black lines in panel a-d and f-i are the DOI.

DISCUSSION

The comparison between the classic Cole-Cole model and the re-parameterizations of the Cole-Cole model has been carried out on both TD and FD IP data, but it is beyond the scope of this study to present a complete comparison of the TD and FD IP methods. In fact, the settings of the TD and FD data generation are selected focusing on getting equivalent acquisition ranges, but a TD/FD comparison study should also take other factors into account, e.g. the acquisition range actually measurable in lab/field. Despite the same number of decades (approximately 3.5 decades) being used for both TD and FD synthetic data generation, we see that the two methods are not focused at the exact same spectral range. Indeed, for $\tau = 0.1s$ (the results presented in this study), we see that the synthetic FD data often resolves the model parameters better than the TD data. However, for $\tau = 1\,s$ the situation is the opposite and the TD data gives the best resolution. With these remarks, the TD and the FD methods show approximately the same improvements with the application of the re-parameterized Cole-Cole models.

The MPA, MIC and MIR models show similar results in terms of uncertainty analysis. However, the MPA modelling has an advantage when compared to the MIC and the MIR parameterizations. Indeed, the φ_{max} parameter directly controls the magnitude of

EAGE Publications B.V., PO Box 59, 3990 DB, Houten, The Netherlands

the IP response, while in the MIC and MIR model the response magnitude depends on the σ''_{max}/σ_0 and ρ''_{min}/ρ_0 ratios, respectively.

On the other hand, many petrophysical relations involving IP properties are expressed in terms of real/imaginary conductivity, for instance the linear relation between the real and imaginary surface conductivity described in Weller et al. (2013) or the relation between hydraulic permeability and real and imaginary conductivity found by Weller et al. (2015). In this respect, the MIC model is more suited for applying petrophysical relations directly from the inversion results. A final consideration can be made about the comparison of field and laboratory IP results. Typically, laboratory IP measurements are carried out in FD, and the results are shown in terms of amplitude/phase and/or real/imaginary conductivity. In this respect, inversions of field data in terms of MPA or MIC models are much easier to compare with laboratory results in comparison to classic Cole-Cole or MIR inversions.

CONCLUSION

We have derived and tested three re-parameterization of the Cole-Cole model for inversion of TDIP and FDIP data, namely the Maximum Phase Angle (MPA) Cole-Cole model $\{\rho_0, \varphi_{\max}, \tau_\varphi, C\}$, the Maximum Imaginary Conductivity (MIC) Cole-Cole model $\{\sigma_0, \sigma''_{max}, \tau_\sigma, C\}$ and the Minimum Imaginary Resistivity (MIR) Cole-Cole model $\{\rho_0, \rho''_{min}, \tau_\rho, C\}$.

The uncertainty analyses of synthetic homogenous half space models and multilayered model, which were computed using MCMC method, show that the MPA, MIC and MIR

EAGE Publications B.V., PO Box 59, 3990 DB, Houten, The Netherlands

Cole-Cole parameters, compared to the classic Cole-Cole parameters, are less correlated in the inversion of both FD and TD IP data. Consequently, we see that the re-parameterizations increase the resolution of the model parameters, specifically of the $\varphi_{\max}$, σ''_{max} and ρ''_{min} parameters in comparison to the classic m_0 parameter. The resolution improvement obtained by the re-parameterizations is especially significant for models with low C values or low signal-to-noise ratio (i.e. models that are poorly resolved using the classic Cole-Cole model), where 3-fold improvements or better are observed. The resolution improvements are less pronounced or absent for models that are well resolved with the classic Cole-Cole model.

A 2D field example where we compare the classic Cole-Cole and the MIC models shows that gradient-based inversion methods benefit from the re-parameterizations as well. A significantly deeper (more than double) depth of investigation was found for σ''_{max} in comparison to the classic m_0, together with a better correlation with geology.

Consequently, it is recommended to invert for one of the re-parameterizations of the Cole-Cole model in any Cole-Cole inversion of IP data and then, if needed, transform the parameters back to the classic parameterization. In particular, we believe that the MPA and the MIC parameterizations will be particularly effective for the spectral inversion of field IP data and will contribute to narrow the gap between IP theory, laboratory findings and field applications.

ACKNOWLEDGMENTS

EAGE Publications B.V., PO Box 59, 3990 DB, Houten, The Netherlands

This work was cofounded by the project GEOCON (Advancing GEOlogical, geophysical and CONtaminant monitoring technologies for contaminated site investigation, www.geocon.env.dtu.dk) .

EAGE Publications B.V., PO Box 59, 3990 DB, Houten, The Netherlands

APPENDIX A

From MPA Cole-Cole to classic Cole-Cole

Given the MPA Cole-Cole model parameters $\{\rho_0, \varphi_{\max}, \tau_\varphi, C\}$, the corresponding parameters of the resistivity (or conductivity) Cole-Cole model $\{\rho_0, m_0, \tau_\rho, C\}$ can be computed through the following iterative approach.

As a start, we define the variables a and b as:

$$a(\omega) = Re\left(\frac{1}{1+(i\omega\tau_\rho)^C}\right) \quad \text{(A.1)}$$

$$b(\omega) = Im\left(\frac{1}{1+(i\omega\tau_\rho)^C}\right) \quad \text{(A.2)}$$

where Re and Im indicate the computation of the real and imaginary part of a complex number, respectively. Thus, equation 1 can be written as

$$\tilde{\rho}(\omega) = \rho_0\left[1 - m_0\left(1 - \left(a(\omega) + ib(\omega)\right)\right)\right]. \quad \text{(A.3)}$$

We now iterate to minimize

$$\Delta m_0 = \frac{|m_0(n) - m_0(n-1)|}{m_0(n)}, \quad \text{(A.4)}$$

where $m_0(0) = 0$. For the $n'th$ iteration, $\tau_\rho(n)$ and $m_0(n)$ are computed as:

$$\tau_\rho(n) = \tau_\varphi \cdot \left(1 - m_0(n-1)\right)^{-1/2C} \quad \text{(A.5)}$$

$$a(n) = Re\left(\frac{1}{1+\left(i\frac{\tau_\rho(n)}{\tau_\varphi}\right)^C}\right) \quad \text{(A.6)}$$

EAGE Publications B.V., PO Box 59, 3990 DB, Houten, The Netherlands

$$b(n) = Im\left(\frac{1}{1+\left(i\frac{\tau_\rho(n)}{\tau_\varphi}\right)^C}\right) \quad \text{(A.7)}$$

$$m_0(n) = \frac{tan(-\varphi_{max})}{(1-a(n))\cdot tan(-\varphi_{max})+b(n)}. \quad \text{(A.7)}$$

Once the classic Cole-Cole parameters $\{\rho_0, m_0, \tau_\rho, C\}$ are defined in terms of the MPA parameters $\{\rho_0, \varphi_{\max}, \tau_\varphi, C\}$, the Cole-Cole complex resistivity (or conductivity) can be computed through equation 1 (or equation 3) at any frequency.

From MIC Cole-Cole to classic Cole-Cole

Given the MIC Cole-Cole model parameters $\{\sigma_0, \sigma''_{max}, \tau_\sigma, C\}$, the corresponding parameters of the resistivity (or conductivity) Cole-Cole model $\{\rho_0, m_0, \tau_\rho, C\}$ can be computed directly.

As a start, we define the variable d as:

$$d = Im\left(\frac{1}{1+(1i)^C}\right) \quad \text{(A.8)}$$

The chargeability of the Cole-Cole model, m_0, is then given as

$$m_0 = \frac{\sigma''_{max}}{(\sigma''_{max}-\sigma_0\cdot d)}. \quad \text{(A.9)}$$

The relaxation time in the resistivity form, τ_ρ, can now be computed from equation (5)

From MIR Cole-Cole to classic Cole-Cole

Given the MIR Cole-Cole model parameters $\{\rho_0, \rho''_{min}, \tau_\rho, C\}$, the corresponding parameters of the resistivity (or conductivity) Cole-Cole model $\{\rho_0, m_0, \tau_\rho, C\}$ can be computed directly:

EAGE Publications B.V., PO Box 59, 3990 DB, Houten, The Netherlands

$$m_0 = -\frac{\rho''_{min}}{(\rho_0 \cdot d)}, \quad \text{(A.10)}$$

where d is as defined in equation A8.

APPENDIX B

Gating of TDIP signal

The gating of the transient IP signal, which is recorded from 2.6 ms to 12,000 ms, is listen in Table A.1

Table A.1: IP gating

Gate	**1**	**2**	**3**	**4**	**5**	**6**	**7**	**8**	**9**
Gate width (ms)	1.06	1.33	2.13	2.93	4	5.33	7.46	10.4	14.4
Gate	**10**	**11**	**12**	**13**	**14**	**15**	**16**	**17**	**18**
Gate width (ms)	20	20	40	60	80	100	140	200	280
Gate	**19**	**20**	**21**	**22**	**23**	**24**	**25**	**26**	
Gate width (ms)	380	540	760	1040	1460	2020	2800	2000	

Acquisition frequencies

The frequencies used for computation of synthetic frequency-domain IP forward responses.

Table A.2: Acquisition frequencies

Frequencies (Hz)												
0.08	0.16	0.32	0.64	1.28	2.56	5.12	10.2	20.4	40.9	81.9	163	327

EAGE Publications B.V., PO Box 59, 3990 DB, Houten, The Netherlands

REFERENCES

AUKEN, E., CHRISTIANSEN, A. V., JACOBSEN, B. H., FOGED, N. & SØRENSEN, K. I. 2005. Piecewise 1D Laterally Constrained Inversion of resistivity data. *Geophysical Prospecting,* 53**,** 497-506.

BÉRUBÉ, C. L., CHOUTEAU, M., SHAMSIPOUR, P., ENKIN, R. J. & OLIVO, G. R. 2017. Bayesian inference of spectral induced polarization parameters for laboratory complex resistivity measurements of rocks and soils. *Computers & Geosciences,* 105**,** 51-64.

BINLEY, A., SLATER, L. D., FUKES, M. & CASSIANI, G. 2005. Relationship between spectral induced polarization and hydraulic properties of saturated and unsaturated sandstone. *Water Resources Research,* 41**,** 1-13.

BÖRNER, F. D., SCHOPPER, J. R. & WELLER, A. 1996. Evaluation of transport and storage properties in the soil and groundwater zone from induced polarization measurements. *Geophysical Prospecting,* 44**,** 583-601.

CHEN, J., KEMNA, A. & HUBBARD, S. S. 2008. A comparison between Gauss-Newton and Markov-chain Monte Carlo-based methods for inverting spectral induced-polarization data for Cole-Cole parameters. *Geophysics,* 73**,** F247-F259.

COLE, K. S. & COLE, R. H. 1941. Dispersion and absorption in dielectrics. *Journal of Chemical Physics,* 9**,** 341-351.

FIANDACA, G., AUKEN, E., GAZOTY, A. & CHRISTIANSEN, A. V. 2012. Time-domain induced polarization: Full-decay forward modeling and 1D laterally constrained inversion of Cole-Cole parameters. *Geophysics,* 77**,** E213-E225.

FIANDACA, G., CHRISTIANSEN, A. & AUKEN, E. Depth of investigation for multi-parameters inversions. Near Surface Geoscience 2015-21st European Meeting of Environmental and Engineering Geophysics, 2015.

FIANDACA, G., RAMM, J., BINLEY, A., GAZOTY, A., CHRISTIANSEN, A. V. & AUKEN, E. 2013. Resolving spectral information from time domain induced polarization data through 2-D inversion. *Geophysical Journal International,* 192**,** 631-646.

GAZOTY, A., FIANDACA, G., PEDERSEN, J., AUKEN, E. & CHRISTIANSEN, A. V. 2012. Mapping of landfills using time-domain spectral induced polarization data: The Eskelund case study. *Near Surface Geophysics,* 10**,** 575-586.

HASTINGS, W. K. 1970. Monte Carlo sampling methods using Markov chains and their applications. *Biometrika,* 57**,** 97-109.

HÖNIG, M. & TEZKAN, B. 2007. 1D and 2D Cole-Cole-inversion of time-domain induced-polarization data. *Geophysical Prospecting,* 55**,** 117-133.

JOHANSSON, S., FIANDACA, G. & DAHLIN, T. 2015. Influence of non-aqueous phase liquid configuration on induced polarization parameters: Conceptual models applied to a time-domain field case study. *Journal of Applied Geophysics,* 123**,** 295-309.

JOHANSSON, S., SPARRENBOM, C., FIANDACA, G., LINDSKOG, A., OLSSON, P.-I., DAHLIN, T. & ROSQVIST, H. 2016. Investigations of a Cretaceous limestone with spectral induced polarization and scanning electron microscopy. *Geophysical Journal International***,** ggw432.

KEMNA, A., BINLEY, A. & SLATER, L. 2004. Crosshole IP imaging for engineering and environmental applications. *Geophysics,* 69**,** 97-107.

EAGE Publications B.V., PO Box 59, 3990 DB, Houten, The Netherlands

LEROUX, V., DAHLIN, T. & SVENSSON, M. 2007. Dense resistivity and induced polarization profiling for a landfill restoration project at Härlöv, Southern Sweden. *Waste Management & Research,* 25**,** 49-60.

LOKE, M. H., CHAMBERS, J. E. & OGILVY, R. D. 2006. Inversion of 2D spectral induced polarization imaging data. *Geophysical Prospecting,* 54**,** 287-301.

MADSEN, L. M., FIANDACA, G., AUKEN, E. & CHRISTIANSEN, A. V. 2017. Time-domain induced polarization - an analysis of Cole-Cole parameter resolution and correlation using Markov Chain Monte Carlo inversion. *Geophysical Journal International*.

MALINVERNO, A. 2002. Parsimonious Bayesian Markov chain Monte Carlo inversion in a nonlinear geophysical problem. *Geophysical Journal International,* 151**,** 675-688.

MAURYA, P. K., FIANDACA, G., AUKEN, E. & CHRISTIANSEN, A. V. Lithological characterization of a comtaminated site using direct current resistivity and time domain induced polarization. IP2016/4th International Workshop on Induced Polarization, 6.-8. June 2016 2016 Aarhus, Denmark.

METROPOLIS, N., ROSENBLUTH, A. W., ROSENBLUTH, M. N., TELLER, A. H. & TELLER, E. 1953. Equation of state calculations by fast computing machines. *The journal of chemical physics,* 21**,** 1087-1092.

MOSEGAARD, K. & TARANTOLA, A. 2002. Probabilistic Approach to Inverse Problems. *In:* W. LEE, P. J., C. KISSLINGERS, AND H. KANAMORI (ed.) *International handbook of earthquake and engineering seismology.* Academic Press.

NORDSIEK, S., DIAMANTOPOULOS, E., HÖRDT, A. & DURNER, W. 2016. Relationships between soil hydraulic parameters and induced polarization spectra. *Near Surface Geophysics,* 14**,** 23-37.

OLSSON, P.-I., FIANDACA, G., LARSEN, J. J., DAHLIN, T. & AUKEN, E. 2016. Doubling the spectrum of time-domain induced polarization by harmonic de-noising, drift correction, spike removal, tapered gating and data uncertainty estimation. *Geophysical Journal International,* 207**,** 774-784.

OLSSON, P. I., DAHLIN, T., FIANDACA, G. & AUKEN, E. 2015. Measuring time-domain spectral induced polarization in the on-time:decreasing acquisition time and increasing signal-to-noise ratio. *Journal of Applied Geophysics,* 2015**,** 6.

PELTON, W. H., WARD, S. H., HALLOF, P. G., SILL, W. R. & NELSON, P. H. 1978. Mineral discrimination and removal of inductive coupling with multifrequency IP. *Geophysics,* 43**,** 588-609.

SEIGEL, H. O. 1959. Mathematical Formulation and type curves for induced polarization. *Geophysics,* 24**,** 547-565.

SLATER, L. D. & LESMES, D. 2002. IP interpretation in environmental investigations. *Geophysics,* 67**,** 77-88.

TARASOV, A. & TITOV, K. 2013. On the use of the Cole–Cole equations in spectral induced polarization. *Geophysical Journal International,* 195**,** 352-356.

VANHALA, H. 1997. Mapping oil-contaminated sand and till with the spectral induced polarization (IP) method. *Geophysical Prospecting,* 45**,** 303-326.

WELLER, A., SLATER, L., BINLEY, A., NORDSIEK, S. & XU, S. 2015. Permeability prediction based on induced polarization: Insights from measurements on sandstone and unconsolidated samples spanning a wide permeability range. *Geophysics,* 80**,** D161-D173.

WELLER, A., SLATER, L. & NORDSIEK, S. 2013. On the relationship between induced polarization and surface conductivity: Implications for petrophysical interpretation of electrical measurements. *Geophysics,* 78**,** D315-D325.

YOSHIOKA, K. & ZHDANOV, M. S. 2005. Three-dimensional nonlinear regularized inversion of the induced polarization data based on the Cole-Cole model. *Physics of the Earth and Planetary Interiors,* 150**,** 29-43.

YUVAL & OLDENBURG, D. W. 1997. Computation of Cole-Cole parameters from IP data. *Geophysics,* 62**,** 436-448.

Re-parameterizations of the Cole-Cole model for improved spectral inversion of induced polarization data

Gianluca Fiandaca*, Line Meldgaard Madsen*, Pradip Kumar Maurya*

*HydroGeophysics Group, Department of Geoscience, Aarhus University,

C.F. Møllers Alle 4, DK-8000 Aarhus C, Denmark

Short title: Re-parameterization of Cole-Cole model

Date of first submission: 31.01.2017

Resubmission: 20.09.2017

Corresponding author: Line Meldgaard Madsen, linemeldgaad@geo.au.dk

ABSTRACT

The induced polarization phenomenon, both in time-domain (TD) and frequency-domain (FD), is often parameterized using the empirical Cole-Cole model. To improve the resolution of model parameters and to decrease the parameter correlations in the inversion process of induced polarization data, we here suggest three re-parametrizations of the Cole-Cole model, namely the Maximum Phase Angle (MPA) Cole-Cole model, the Maximum Imaginary Conductivity (MIC) Cole-Cole model and the Minimum Imaginary Resistivity (MIR) Cole-Cole model. The MPA Cole-Cole model uses the maximum phase φ_{max} and the inverse of the phase peak frequency, τ_{φ}, instead of the intrinsic chargeability m_0 and the time constant adopted in the classic Cole-Cole model; the MIC Cole-Cole model uses the maximum imaginary conductivity σ''_{max} instead of the m_0, and the time constant τ_{σ} of the Cole-Cole model in its conductivity form; the MIR Cole-Cole model uses the minimum imaginary resistivity ρ''_{min} instead of the m_0, and the time constant τ_{ρ} of the Cole-Cole model in its resistivity form.

The effects of the three re-parameterizations have been tested on synthetic TD and FD data using a Markov Chain Monte Carlo inversion method, which allows for easy quantification of parameter uncertainty, and on field data using 2D gradient-based inversion. In comparison with the classic Cole-Cole model, it was found that for all the three re-parameterizations the model parameters are less correlated with each other and, consequently, better resolved for both TD and FD data. The increase in model resolution is particularly significant for models that are poorly resolved using the classic Cole-Cole parameterization, for instance for low values of the frequency exponent or with

EAGE Publications B.V., PO Box 59, 3990 DB, Houten, The Netherlands

low signal-to-noise ratio. In general, this leads to a significantly deeper depth of investigation for the φ_{max}, σ''_{max} and ρ''_{min} parameters, when compared to the classic m_0 parameter, which is shown with a field example. We believe that the use of the re-parameterizations for inverting field data will contribute to narrow the gap between IP theory, laboratory findings and field applications.

INTRODUCTION

The induced polarization (IP) method is a geophysical technique providing direct sensitivity to the electrical properties of the subsurface at the interface between the rock matrix and the wetting fluid. The method was originally used for mineral exploration, but, today, it is frequently applied in environmental surveys where the applications include mapping and characterization of lithology and soil-types (e.g. Slater and Lesmes, 2002, Kemna et al., 2004, Maurya et al., 2016, Johansson et al., 2016) and characterization of contaminated sites and landfills (e.g. Vanhala, 1997, Leroux et al., 2007, Gazoty et al., 2012, Johansson et al., 2015). Studies have also been investigating the link between the IP effect and hydraulic properties of the subsurface (e.g. Börner et al., 1996, Binley et al., 2005, Weller et al., 2015, Nordsiek et al., 2016).

In time-domain (TD), the IP phenomenon manifests itself as a transient potential rise/decay following the switch on/off of an electric current induced through a medium. In frequency-domain (FD), this corresponds to a phase shift between the applied current and the arising potential. The IP effect of a material can thus be described by a frequency-dependent complex electrical resistivity. However, no universal physical model is available to describe the effect, why IP often is parameterized using phenomenological models.

The classic Debye model describes the simplest form of a dielectric relaxation response to an alternating current. Cole and Cole (1941) extended the Debye model to account for new experimental observations on different materials. The original Cole-Cole model, expressed in terms of a complex dielectric constant, was later rewritten by Pelton

EAGE Publications B.V., PO Box 59, 3990 DB, Houten, The Netherlands

et al. (1978) to describe the complex resistivity response of mineralized rocks. A complex conductivity form of the original Cole-Cole model is often encountered in literature as well (e.g. Tarasov and Titov, 2013).

Today, the Cole-Cole model (in resistivity or conductivity form) is one of the most prevailing models used for parameterization and inversion of TD IP data (e.g. Yuval and Oldenburg, 1997, Hönig and Tezkan, 2007, Fiandaca et al., 2012) as well as FD IP data (e.g. Yoshioka and Zhdanov, 2005, Loke et al., 2006).

Madsen et al. (2017) presented a sensitivity analysis of Cole-Cole parameters retrieved from TD IP data. In this study, the Cole-Cole model (resistivity form) was used in terms of the following parameters: the direct current resistivity (ρ_0), the intrinsic chargeability (m_0) as described by Seigel (1959), the relaxation time (τ_ρ) and the frequency exponent (C). Here, the τ_ρ symbol is used instead of the classic τ symbol for stressing the fact that τ_ρ refers to the resistivity Cole-Cole model.

The sensitivity analysis proved that spectral Cole-Cole parameters can be retrieved from TD IP data when using full-decay data and an acquisition range above 2.5 decades in time, but that the resolution of the Cole-Cole parameters decreases significantly for small values of C and for values of τ_ρ far outside the acquisition range (Madsen et al., 2017). Furthermore, a strong correlation between m_0 and C was detected in both synthetic generated data and field data. The correlation between m_0 and C have also been detected from inversion of FD IP data (Bérubé et al., 2017).

To improve the model resolution retrieved from inversion of IP data, we suggest three re-parametrizations of the Cole-Cole model: The Maximum Phase Angle (MPA) Cole-Cole, the Maximum Imaginary Conductivity (MIC) Cole-Cole model and the Minimum

EAGE Publications B.V., PO Box 59, 3990 DB, Houten, The Netherlands

Imaginary Resistivity (MIR) Cole-Cole model. The sensitivity of the classic and the new Cole-Cole model parameters are compared using Markov Chain Monte Carlo (MCMC) inversion, which allows us to study the posterior probability distributions of each parameter and quantify uncertainties without linearization. We show that models, which are poorly resolved from inversion with the classic Cole-Cole model (e.g. due to low signal-to-noise ratio) can be resolved well with the new re-parameterizations and that the re-parameterizations work equally well for TD and FDIP data. In addition, we present a field example that shows that gradient-based inversions benefits from the re-parameterizations as well and consequently obtain a significantly deeper depth of investigation.

RE-PARAMETRIZATIONS OF COLE-COLE

The Cole-Cole model describing the complex resistivity is defined as (Pelton et al., 1978)

$$\tilde{\rho}(\omega) = \rho'(\omega) + i\rho''(\omega) = \rho_0\left[1 - m_0\left(1 - \frac{1}{1+(i\omega\tau_\rho)^C}\right)\right], \quad (1)$$

where ρ_0, m_0, τ_ρ, and C are the previously described Cole-Cole parameters, $\omega = 2\pi f$ is the angular frequency, and i is the imaginary unit. The model space is thus defined as

$$\boldsymbol{m}_{\boldsymbol{resistivity\ Cole-Cole}} = \{\rho_0, m_0, \tau_\rho, C\}. \quad (2)$$

Alternatively, the Cole-Cole model can also be presented in its conductivity form (e.g. Tarasov and Titov, 2013),

EAGE Publications B.V., PO Box 59, 3990 DB, Houten, The Netherlands

$$\tilde{\sigma}(\omega) = \sigma'(\omega) + i\sigma''(\omega) = \sigma_0 \left[1 - \frac{m_0}{1-m_0}\left(1 - \frac{1}{1+(i\omega\tau_\sigma)^C}\right)\right], \quad (3)$$

with the corresponding model space defined as

$$\boldsymbol{m}_{\textbf{conductivity Cole–Cole}} = \{\sigma_0, m_0, \tau_\sigma, C\}. \quad (4)$$

The conductivity and resistivity Cole-Cole models (CCC and RCC) are identical, i.e. $\tilde{\sigma}(\omega) = 1/\tilde{\rho}(\omega)$, when the respective relaxation times τ_σ and τ_ρ obey the following relation:

$$\tau_\sigma = \tau_\rho \cdot (1 - m_0)^{1/C}. \quad (5)$$

The inverse of τ_σ represents the angular frequency of the maximum of the imaginary conductivity,

$$\sigma''_{max} = \sigma''(\omega = 1/\tau_\sigma), \quad (6)$$

while the inverse of τ_ρ represents the angular frequency of the minimum of the imaginary resistivity,

$$\rho''_{min} = \rho''(\omega = 1/\tau_\rho). \quad (7)$$

Fig. 1 shows the absolute value of the complex resistivity $|\tilde{\rho}|$, the phase of the complex conductivity φ, the imaginary conductivity σ'' and the imaginary resistivity ρ'' of the Cole-Cole model as a function of frequency for the model defined by $\rho_0 = 100\ \Omega m$, $m_0 = 500\ mV/V$, $\tau_\rho = 0.1\ s$ and $C = 0.2$. The high m_0-value was chosen to emphasize the frequency variation of the spectrum.

The phase of the complex conductivity, $\varphi(\omega)$ (Fig. 1b), can be defined both in terms of equation 1 and equation 3, so

EAGE Publications B.V., PO Box 59, 3990 DB, Houten, The Netherlands

$$\varphi(\omega) = tan^{-1}\left(\frac{\sigma''(\omega)}{\sigma'(\omega)}\right) = -tan^{-1}\left(\frac{\rho''(\omega)}{\rho'(\omega)}\right). \quad (8)$$

The phase reaches a maximum, φ_{max}, at an angular frequency $\omega_\varphi = 1/\tau_\varphi$ (Fig 1b),

$$\varphi_{max} = tan^{-1}\left(\frac{\sigma''\left(1/\tau_\varphi\right)}{\sigma'\left(1/\tau_\varphi\right)}\right) = -tan^{-1}\left(\frac{\rho''\left(1/\tau_\varphi\right)}{\rho'\left(1/\tau_\varphi\right)}\right), \quad (9)$$

where the relaxation time, τ_φ, is linked to τ_ρ and τ_σ through the other Cole-Cole parameters m_0 and C:

$$\tau_\varphi = \tau_\rho \cdot (1 - m_0)^{1/2C} = \tau_\sigma \cdot (1 - m_0)^{-1/2C}. \quad (10)$$

The differences between τ_ρ, τ_σ and τ_φ increase with an increase of m_0 and/or with a decrease of C. Furthermore, φ_{max}, as well as σ''_{max} and ρ''_{min}, increases with m_0 and C. The dependence of the phase shift on both m_0 and C is the main reason for the parameter correlations described by Madsen et al. (2017) and Bérubé et al. (2017), as depicted in Fig. 2. In fact, with frequency ranges below 4 decades, which is typical in field IP surveying, similar variations in the phase spectrum can be induced by decreasing m_0 (magenta line, Fig. 2a) or C (blue line, Fig. 2a). A similar equivalence is found in TD, with acquisition ranges below 4 decades (Fig. 2b). However, it has to be noted that in order to take the acquisition range in the TD forward response into account, the current waveform, and in particular the duration of the current injection, has to be modelled. This explains the difference between the step response (dashed black line) and the response with limited acquisition range (continuous black line) in Fig. 2b.

EAGE Publications B.V., PO Box 59, 3990 DB, Houten, The Netherlands

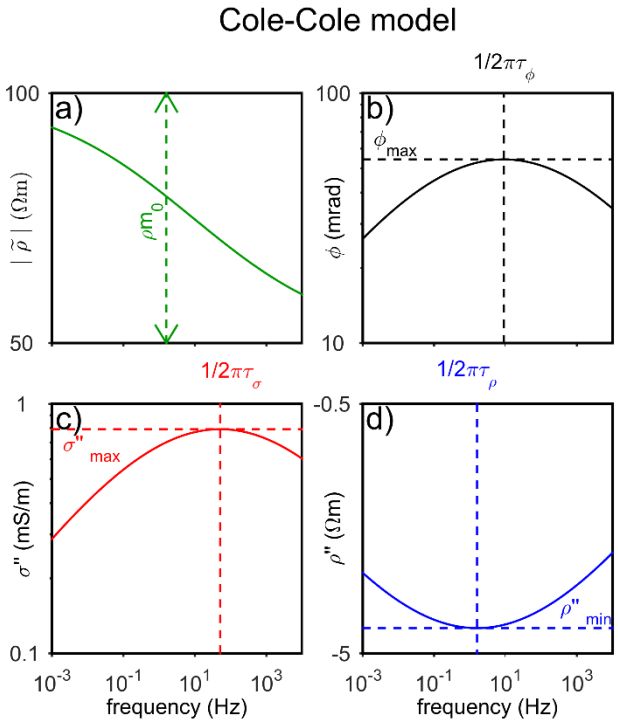

Figure 1. *Cole-Cole model defined by* $\rho_0 = 100\,\Omega m$, $m_0 = 500\,mV/V$, $\tau_\rho = 0.1\,s$, *and* $C = 0.2$. *a) amplitude of the complex resistivity; b) phase of the complex conductivity; c) imaginary conductivity; d) imaginary resistivity.*

EAGE Publications B.V., PO Box 59, 3990 DB, Houten, The Netherlands

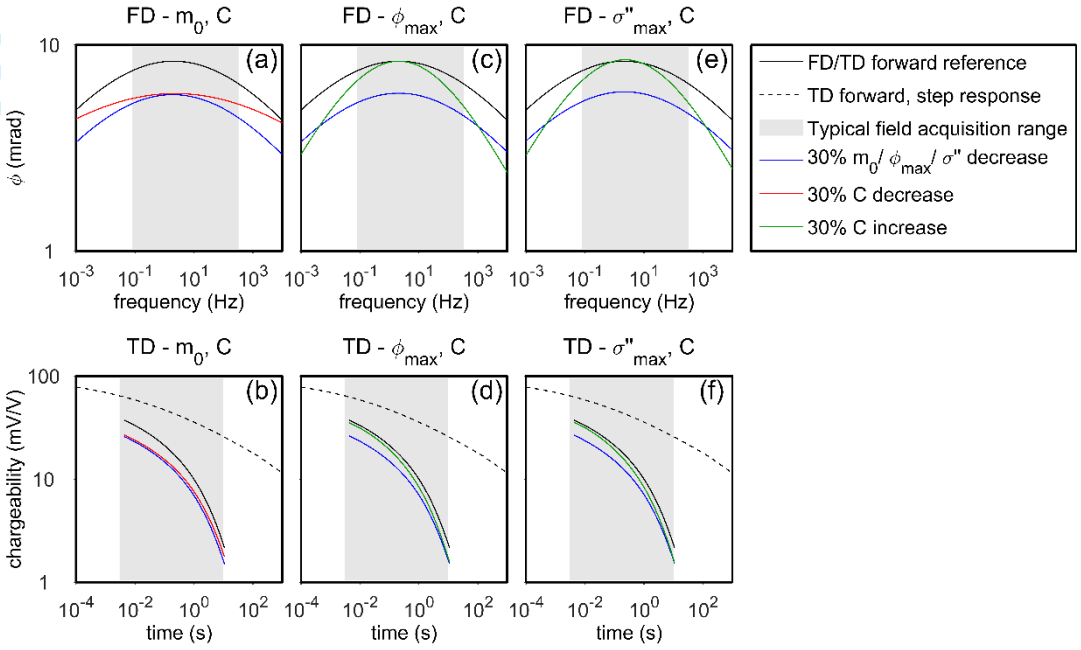

Figure 2. *Variations of frequency-domain (FD) and time-domain (TD) responses with* $m_0, \varphi_{max}, \sigma''_{max}$ *and* C*. Reference model:* $\rho_0 = 100\ \Omega m$, $m_0 = 100\ mV/V$, $\tau_\rho = 0.1\ s$, *and* $C = 0.2$. *a) FD responses,* m_0 *and* C *variations; b) TD responses,* m_0 *and* C *variations; c) FD responses,* φ_{max} *and* C *variations; d) TD responses,* φ_{max} *and* C *variations; e) FD responses,* σ''_{max} *and* C *variations; f) TD responses,* σ''_{max} *and* C *variations.*

Maximum Phase Angle (MPA)

We suggest a re-parameterization of the Cole-Cole model where instead of m_0 and τ_ρ the maximum phase $\varphi_{\max}$ (equation 9 and Fig. 1b) and the phase relaxation time τ_φ (equation 10 and Fig. 1b) are used as model parameters. The re-parameterized model space becomes:

$$\boldsymbol{m}_{\boldsymbol{MPA\ Cole-Cole}} = \{\rho_0, \varphi_{\max}, \tau_\varphi, C\}. \quad (11)$$

EAGE Publications B.V., PO Box 59, 3990 DB, Houten, The Netherlands

In Fig. 2c the variations in the phase spectrum induced by a decrease of $\varphi_{\max}$ (blue line) and an increase of C (green line) are shown. In comparison to the classic Cole-Cole parameterization (Fig. 2a), a much bigger data difference is present between the responses, meaning that $\varphi_{\max}$ and C are less correlated than m_0 and C. The same applies in the comparison of the TD responses in Fig. 2b and Fig. 2d. In TD, we see that the green response (C 30% decrease) follows the reference model at the early time and the blue response ($\varphi_{\max}$ 30% decrease) at the late times (Fig. 2d).

To summarize, the parameter $\varphi_{\max}$ controls the FD maximum phase shift, as well as the magnitude of the TD decays, while the parameter C controls the width of the phase shift and the decay shape.

Given the MPA Cole-Cole model parameters $\{\rho_0, \varphi_{\max}, \tau_\varphi, C\}$, the corresponding parameters of the RCC (or CCC) model $\{\rho_0, m_0, \tau_\rho, C\}$ can be easily computed through an iterative approach (See Appendix A).

Maximum Imaginary Conductivity (MIC)

Another re-parameterization of the classic Cole-Cole model is the Maximum Imaginary Conductivity (MIC) Cole-Cole model. The MIC model space is defined in terms of

$$\boldsymbol{m}_{\boldsymbol{MIC\ Cole-Cole}} = \{\sigma_0, \sigma''_{max}, \tau_\sigma, C\}, \quad (12)$$

where σ''_{max} is the maximum of the imaginary conductivity (Fig. 1c) as defined as in equation 6.

The influence of changes in σ''_{max} and C on the phase shift and the chargeability is shown in Fig. 2e and Fig. 2f, respectively. The responses are very similar to those of $\varphi_{\max}$, because $\sigma''_{max} \cong \sigma_0 \varphi_{\max}$. Given the MIC Cole-Cole model parameters, the

EAGE Publications B.V., PO Box 59, 3990 DB, Houten, The Netherlands

corresponding parameters of the CCC models can be computed directly as shown in Appendix A.

Minimum Imaginary Resistivity (MIR)

The resistivity equivalence to the MIC Cole-Cole model is the Minimum Imaginary Resistivity (MIR) Cole-Cole model. The model space is defined in terms of

$$\boldsymbol{m}_{\boldsymbol{MIR\ Cole-Cole}} = \{\rho_0, \rho''_{min}, \tau_\rho, C\}, \quad (13)$$

where ρ''_{min} is the minimum of the imaginary resistivity (Fig. 1d) as defined in equation 7. The responses of the MIR Cole-Cole model are not shown in Fig. 2 as they are similar to those of $\varphi_{\max}$ and σ''_{max}, because $\rho''_{min} \cong -\rho_0\varphi_{\max}$.

Given the MIR Cole-Cole model parameters, the corresponding parameters of the RCC model can be computed directly as shown in Appendix A.

DATA SPACE

Time-domain data

The data space, d_{obs}, for the MCMC and gradient-based inversions of TD IP data consists of apparent resistivity and full-decay chargeability values:

$$\boldsymbol{d}_{\boldsymbol{obs}} = \{\rho_a, M_i\}, i = 1{:}\,N_{gates} \quad (14)$$

where ρ_a (Ωm) is the apparent resistivity and the data-space chargeability, M_i (mV/V), is computed in each time-gate, i, of the transient full-decay IP signal as described by

EAGE Publications B.V., PO Box 59, 3990 DB, Houten, The Netherlands

Olsson et al. (2015). If no negative data are present, the inversion can be performed in logarithmic data space.

A waveform with a 100% duty cycle, where the TD IP data are measured in the current-on time as described by Olsson et al. (2015), is applied for both generation of synthetic data and in the field data acquisition. For the synthetic data, each IP signal is recorded from 2.6 ms to 12,000 ms and the decay is divided into 26 time-gates (listed in Appendix B) with an approximately log-increasing gate width to improve the signal-to-noise ratio at late times (Fiandaca et al., 2012). The same acquisition range (about 3.5 decades) is also obtainable in field surveying when full-waveform recordings are processed for harmonic de-noising and background removal (see details in the field example). Three stacks have been model in the synthetic forward responses, while two stacks have been used in the field example. The used quadrupoles and the noise model are described in the separate results section for the synthetic data and field data.

Frequency-domain data

For the FD IP data, the data space consists of the amplitude, A_j (Ωm), and the data-space phase, φ_j (mrad), which are measured at a range of frequencies, j. Similarly to the phase defined in model space, the data space phase is defined here as the phase of the complex conductivity. The data vector applied in the inversion becomes:

$$\boldsymbol{d_{obs}} = \{\varphi_j, A_j\}, j = 1{:}\, N_{frequencies} \quad (15)$$

For the synthetic data, we simulate measurements at 13 frequencies in the range from 0.08 Hz to 327 Hz and thereby get 26 data values in total, the same as the number of time-gates applied in TD. In total, about 3.5 decades in frequency are spanned by the data, with first and last frequency approximately equal to the inverse of the last and first

EAGE Publications B.V., PO Box 59, 3990 DB, Houten, The Netherlands

TD center gate time, respectively. The applied frequencies are listed in Appendix B. Used quadrupoles and noise model are described in the result section.

INVERSION METHODOLOGY

The 1D TD forward response of synthetic data is computed using the algorithm presented in Fiandaca et al. (2012). This algorithm computes the full-decay IP response and models the transmitter current waveform and the receiver transfer function accurately. The same algorithm has been applied to compute the FD forward response by disregarding the time-domain transform. An extension of the algorithm, which computes the 2D forward response (Fiandaca et al., 2013), has been applied in the inversion of field data.

In the following analyses of the re-parameterizations of the Cole-Cole model, we have used two different inversion methods. First, a MCMC inversion algorithm is used to compute a non-linearized uncertainty analysis of all the model parameters. Hereafter, a field example is inverted in 2D using a gradient-based inversion approach in order to show how field surveys may benefit from the re-parameterizations.

MCMC inversion

With the MCMC inversion method, it is possible to investigate the distribution of models that fit a given data set. Compared to a gradient-based inversion, the MCMC method (as well as other statistical inversion approaches) has an advantage when it comes to quantifying parameter uncertainties and correlations without linearizing the problem as described by Chen et al. (2008) and Madsen et al. (2017).

EAGE Publications B.V., PO Box 59, 3990 DB, Houten, The Netherlands

In this study, we apply a Metropolis-Hastings sampling algorithm (Metropolis et al., 1953, Hastings, 1970) that, based on a random-walk in the model space, samples models according to their likelihood. The sampled models make up a Markov Chain, which converges toward the posterior probability distribution of the model space.

The applied sampling algorithm, which is described in details in Madsen et al. (2017), works in two steps. First, a model is proposed. Next, the model is accepted to the Markov Chain with an acceptance probability that depends only on the last accepted model in the chain and none of the previous models. These two steps are repeated a predefined number of times or until the distribution of the sampled models (the posterior probability distribution) has converged.

Because we apply a symmetric model proposer, where the possibility of walking from model $\boldsymbol{m_i}$ to $\boldsymbol{m_j}$ is the same as walking from $\boldsymbol{m_j}$ to $\boldsymbol{m_i}$, the acceptance probability of $\boldsymbol{m_i}$ can be computed simply as a likelihood ratio (Malinverno, 2002):

$$P_{acc}(\boldsymbol{m_i}) = min\left[1, \frac{P_{like}(\boldsymbol{m_i})}{P_{like}(\boldsymbol{m_{i-1}})}\right], \tag{16}$$

where the likelihood function is given as by Mosegaard and Tarantola (2002):

$$P_{like}(\boldsymbol{m}) = k \cdot \exp\left[\frac{1}{2}(g(\boldsymbol{m}) - \boldsymbol{d_{obs}})^T \boldsymbol{C_{obs}}(g(\boldsymbol{m}) - \boldsymbol{d_{obs}})\right], \tag{17}$$

where $g(\boldsymbol{m})$ is the forward response of the model $\boldsymbol{m}$, $\boldsymbol{C_{obs}}$ is the covariance matrix of the observed data, $\boldsymbol{d_{obs}}$, and k is a normalization constant.

Due to the logarithmic transform applied on the model parameters, uncertainties are given as standard deviation factors (STDFs), where the STDF of the marginal posterior probability distribution, PDF (defined in the logarithmic space), can be computed as

EAGE Publications B.V., PO Box 59, 3990 DB, Houten, The Netherlands

$$STDF = exp(STD(PDF)). \quad (18)$$

Assuming the model parameters to be normally distributed in the logarithmic space, the ±STD limits are given by

$$\frac{\mu}{STDF} < \mu < \mu \cdot STDF, \quad (19)$$

were μ is the mean of the distribution. So, with $STDF$ = 1.1 the model parameter has a relative uncertainty of 10%, while with $STDF$ = 2.0 the uncertainty grows 10-fold to 100%. Using the terminology of Auken et al. (2005), a STDF < 1.2 is a well-resolved parameter, 1.2 < STDF < 1.5 is a moderately resolved parameter, 1.5 < STDF < 2 is a poorly resolved parameter and a STDF > 2 is an unresolved parameter.

The posterior distribution of the classic Cole-Cole parameters is related to the ones of the re-parameterizations. In theory, with a complete knowledge of the posterior distribution of the Cole-Cole model (included the asymptotic behavior) and an analytical expression for the mapping between the parameterizations, it would be possible to obtain the posterior distribution of the re-parameterization from the one of the classic Cole-Cole. This is difficult to obtain in practice, why we have chosen to sample the distributions for each parameterization individually.

Gradient-based inversion

For inversion of field data, we apply the gradient-based 2D inversion scheme that is described in detail by Fiandaca et al. (2013). The algorithm applies the first term Taylor expansion for linearization and uses a iterative method to minimizes the misfit,

$$\chi = \left(\frac{\delta \boldsymbol{d}^T \boldsymbol{C}_{obs}^{-1} \delta \boldsymbol{d} + \delta \boldsymbol{r}^T \boldsymbol{C}_R^{-1} \delta \boldsymbol{r}}{N_d + N_R} \right)^{\frac{1}{2}}, \quad (20)$$

EAGE Publications B.V., PO Box 59, 3990 DB, Houten, The Netherlands

where $\delta \boldsymbol{d}$ is the data misfit, $\boldsymbol{C}_{obs}$ is the covariance matrix of the observed data, $\delta \boldsymbol{r}$ is the model roughness and $\boldsymbol{C}_R$ is the covariance on the roughness constraints. N_d and N_R are the numbers of data parameters and roughness constrains, respectively. No priors have been used in the inversion, however, if priors were applied this would add an extra term to equation 20.

From the inversion result, a linearized uncertainty analysis is computed based on the posterior covariance matrix (Tarantola and Valette, 1982),

$$\boldsymbol{C}_{est} = \left(\boldsymbol{G}^T {\boldsymbol{C}_{obs}}^{-1} \boldsymbol{G} + \boldsymbol{R}^T {\boldsymbol{C}_R}^{-1} \boldsymbol{R}\right)^{-1}, \quad (21)$$

where $\boldsymbol{G}$ is the Jacobian matrix holding the partial derivatives of the mapping and $\boldsymbol{R}$ is the roughness matrix. Equivalent to the uncertainty analysis in the MCMC approach (equation 18 and equation 19), a STDF of the $i'th$ model parameter m_i can then be computed as

$$STDF(m_i) = \exp\left(\sqrt{C_{est(i,i)}}\right). \quad (22)$$

The STDFs computed for the gradient-based inversion (using equation 21 and equation 22) are influenced by the values of the roughness constrains, why they should only be seen as a relative measure of the uncertainty and cannot be directly compared to the STDFs of constraint-free inversions (either MCMC or other gradient-based results).

Alongside the linearized uncertainty analysis in terms of STDFs, the depth of investigation (DOI) of the inversion model is computed. The DOI algorithm used in this study is based on a cumulated approximated analysis (CAA) that incorporates the actual output model from the inversion as well as the data errors, as described in Fiandaca et al. (2015). For a given depth D, the CAA computes the data-driven (i.e. $\boldsymbol{C}_R = 0$ in

EAGE Publications B.V., PO Box 59, 3990 DB, Houten, The Netherlands

equation 21) cumulated uncertainty analysis, model column by model column. This is done by cumulating the sensitivity of all the model cells below the depth D. A threshold value for the STDF of the CAA is defined, and the DOI is computed as the depth at which this threshold is reached. Based on experience, DOI threshold values between 2 and 5 gives reasonable DOI estimations. The values of the DOI threshold are usually increased for the τ parameter, which is significantly less resolved and for which the order of magnitude is of interest even when the parameter resolution is low. In this study, the DOI threshold is STDF = 4 for all parameter except τ, for which STDF = 20. The approximation in the CAA algorithm consists in neglecting the correlations between model parameters belonging to different model columns (lateral data correlation), but still considering the correlation among the Cole-Cole parameters for each model column. This means that the DOI algorithm gives results that depends on the actual model parameterization used in the inversion, and can thus be used as a comparative factor between the parameters of the different Cole-Cole parameterizations.

UNCERTAINTY ANALYSIS

In the following, we presents the results of an uncertainty analysis computed using MCMC methods. The MCMC inversion results are presented as marginal posterior probability distributions, which are the distributions of the sampled models shown for each individual model parameter, and the uncertainty is given as the STDF of each distribution as defined in equation 18.

EAGE Publications B.V., PO Box 59, 3990 DB, Houten, The Netherlands

The applied noise model has a relative and an absolute term, for both TD and FD data. In TD, a 2% standard deviation has been applied to the resistivity data; 10% relative standard deviation plus 0.2 mV/V absolute noise has been applied on the IP data. Similarly, in FD a 2% standard deviation is considered for the amplitude data; 10% relative standard deviation plus 0.2 mrad absolute noise has been applied on the phase data.

A homogenous half space example

Synthetic data have been generated from a homogenous half-space model using one quadrupole with electrode spacing $|AB| = 7.5$ m and $|MN| = 2.5$ m.

Five different parameterizations have been investigated: the classic Cole-Cole model in both conductivity form (CCC) and resistivity form (RCC); the three new re-parameterizations (MPA, MIC, MIR). The values of the parameters for all parameterizations were derived from the CCC model: $\sigma_0 = 10\, mS/m$, $m_0 = 100\, mV/V$, $\tau_\sigma = 0.1\, s$, and $C = 0.2$. MCMC inversions of TD and FD synthetic data were performed for each parameterization individually using five MCMC runs with different starting models and with one million model proposes (iterations) in each run.

For both TD and FD, the inversion results from the CCC model and the MIC Cole-Cole model are presented in Fig. 3. The posterior probability distributions are plotted together with the true model (red line) and the STDFs.

For both TD and FD, the resolution of σ_0, τ_σ and C are the same independent on the parameterization (Fig. 3). However, the resolution of σ''_{max} is significantly better than the resolution of m_0. As given by the STDFs, it is approximately a 3-fold improvement in both TD (from STDF = 1.4 to STDF = 1.12) and FD (from STDF = 1.13 to STDF =

EAGE Publications B.V., PO Box 59, 3990 DB, Houten, The Netherlands

1.04). The results of the MPA and the MIR model are very similar to those of the MIC, why they are not show here, however, the STDF are listed in Table 1. Overall, the results show that the FD data gives a better resolved than the TD data. This it is due to the choice of the relaxation time ($\tau_\sigma = 0.1$). If we instead set $\tau_\sigma = 1$, the TD data give the best resolution (see discussion).

Fig. 4 shows the cross-plots of m_0 and σ''_{max} with the remaining Cole-Cole parameters. A non-linear correlation is present between m_0 and τ_σ (Fig. 4b), while the correlation between σ''_{max} and τ_σ is linear and spans a smaller area of the model space (Fig. 4e). The correlation between C and m_0 or σ''_{max} are both non-linear, but we see that σ''_{max} spans a smaller parameter range. Consequently, σ''_{max} is resolved better than m_0.

EAGE Publications B.V., PO Box 59, 3990 DB, Houten, The Netherlands

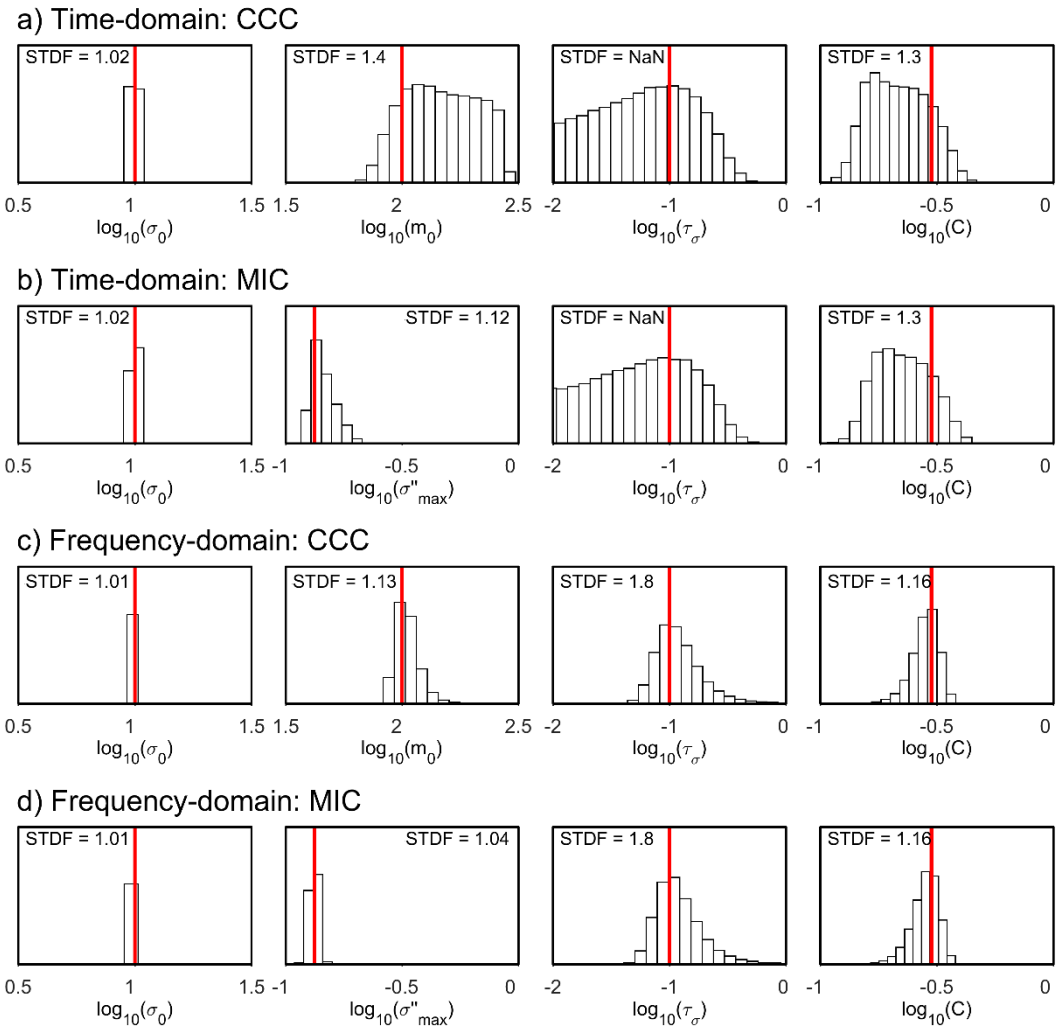

Figure 3. *Posterior probability distributions of a homogenous half space model with the parameters:* $\sigma_0 = 10\ mS/m$, $m_0 = 100\ mV/V$ ($\sigma''_{max} = 0.13\ mS/m$), $\tau_\sigma = 0.1$ *s and* $C = 0.3$. *The distributions are shown for: a) time-domain, conductivity Cole-Cole; b) time-domain, MIC Cole-Cole; c) Frequency-domain, conductivity Cole-Cole; d) frequency-domain, MIC Cole-Cole. The red line marks the true model. NaN indicates that the distribution have not converged. Note that the distributions of* τ_σ *are wider scaled.*

EAGE Publications B.V., PO Box 59, 3990 DB, Houten, The Netherlands

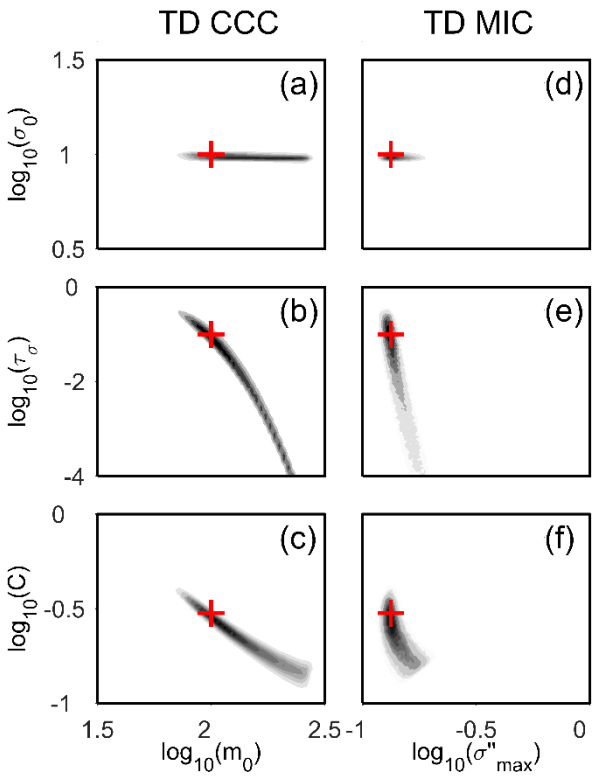

Figure 4. *Cross-plots of the model parameters determined from inversion of time-domain data representing a homogenous half space:* $\sigma_0 = 10\ mS/m$ $m_0 = 100\ mV/V$ $(\sigma''_{max} = 0.13\ mS/m)$, $\tau_\sigma = 0.1\ s$ *and* $C = 0.3$. *Two different models have been used for parameterization of IP: abc) the conductivity Cole-Cole model; def) the MIC Cole-Cole model. The red cross marks the true model.*

Changing the frequency exponent

To study the influence of the re-parameterization on models with different resolutions, the values of C have been varied between $C = 0.2$ and $C = 0.6$ in the CCC model, while the remaining parameters have been kept constant (i.e. $\sigma_0 = 10\ mS/m$, $m_0 = 100\ mV/V$, and $\tau_\sigma = 0.1\ s$). Variation in C in the CCC model gives rise to changes in not just C, but also in σ''_{max}, φ_{max}, ρ''_{min}, τ_φ and τ_ρ in the equivalent re-parameterized models, as these parameters are functions of C and m_0.

EAGE Publications B.V., PO Box 59, 3990 DB, Houten, The Netherlands

As the STDFs of σ_0, ρ_0, τ_φ, τ_σ, τ_ρ and C do not vary significantly between parameterizations (as seen in Fig. 3) and the CCC and RCC results are equivalent, only the STDFs of m_0, φ_{max}, σ''_{max} and ρ''_{min} are presented in the uncertainty analysis in Table 1.

For TD and FD data, the resolution of m_0, φ_{max}, σ''_{max} and ρ''_{min} decreases as the value of C is decreased. For $C = 0.2$, the resolution of φ_{max}, σ''_{max} and ρ''_{min} is close to a 10-fold improvement compared to the resolution of m_0. For $C = 0.4$, the improvement is down to a 2-fold in TD. When $C = 0.6$ the uncertainty is approximately the same for all the parameterizations. This shows that especially poorly resolved models benefit form the re-parameterizations, but the impact on well resolved models is minor.

Table 1: *Uncertainty analysis for different parameterizations for different values of C. Using MCMC inversion, five different models have been analyzed where the value of C has been varied between 0.2 and 0.6 and the remaining parameters have been kept constant:* $\sigma_0 = 10\ mS/m$, $m_0 = 100\ mV/V$, and $\tau_\sigma = 0.1\ s$. *The results are shown from the conductivity Cole-Cole (**m_0**), the MIC Cole-Cole (**σ''_{max}**), the MIR Cole-Cole (**ρ''_{min}**) and the MPA Cole-Cole (**φ_{max}**) parametrization. The uncertainties are given as the STDF of the marginal posterior probability distributions.*

	Time-domain STDFs				**Frequency-domain STDFs**			
C	m_0	σ''_{max}	ρ''_{min}	φ_{max}	m_0	σ''_{max}	ρ''_{min}	φ_{max}
0.2	1.7	1.13	1.12	1.11	1.6	1.06	1.07	1.06
0.3	1.4	1.13	1.12	1.11	1.13	1.04	1.04	1.04
0.4	1.2	1.12	1.10	1.10	1.05	1.04	1.04	1.04
0.5	1.11	1.06	1.06	1.05	1.03	1.04	1.04	1.04
0.6	1.07	1.05	1.05	1.05	1.03	1.04	1.04	1.04

EAGE Publications B.V., PO Box 59, 3990 DB, Houten, The Netherlands

Changing the noise model

In the following, we show the influence of the noise model on the resolution capabilities of the classic Cole-Cole model compared to that of the re-parameterizations. This is done by assuming different noise levels in the data set generated from the previous described model. The noise levels on the FD /TD data-space phase/chargeability values are: 5% relative noise plus 0.1 (mrad for FD and mV/V for TD) absolute noise; 10% relative noise plus 0.2 mrad/mV/V absolute noise (used in the previous examples); 15% relative noise plus 0.3 mrad/mV/V absolute noise.

The results of the uncertainty analysis are presented in Table 2 as the STDFs of the marginal posterior probability distributions of m_0, σ''_{max}, ρ''_{min} and φ_{max}. For all parameterizations, we see that as the noise level is increases, the STDF of the model parameters increases as well. This is also valid for the parameters not shown in the table. The analyses show that the resolution improvements gained from the re-parameterizations, which have been documented in the previous figures, are valid for all the different noise levels. For the low noise level, the improvement is between 3-fold and 4-fold for TD and 2-fold for FD. For the high noise level, the improvement is 2.5-fold in TD and 4-fold in FD. As seen with the example in Fig. 3, the resolution improvement gained with the re-parameterizations is less pronounced for the remaining parameters.

Table 2: *Uncertainty analysis of the influence of three different noise models on the resolution capabilities of the different parameterizations. The model has the parameters:* $\sigma_0 = 10\ mS/m$, $m_0 = 100\ mV/V$, $\tau_\sigma = 0.1\ s$ *and* $C = 0.3$ *The results are shown from the conductivity Cole-Cole* ($\boldsymbol{m_0}$)*, the MIC Cole-Cole* ($\boldsymbol{\sigma''_{max}}$)*, the MIR Cole-Cole* ($\boldsymbol{\rho''_{min}}$) *and the MPA Cole-Cole* ($\boldsymbol{\varphi_{max}}$) *parametrizations. The*

EAGE Publications B.V., PO Box 59, 3990 DB, Houten, The Netherlands

uncertainties are given as the STDF of the marginal posterior probability distributions.

	Time-domain			Frequency-domain		
Noise	**5% 0.1 mV/V**	**10% 0.2 mV/V**	**15% 0.3 mV/V**	**5% 0.1 mrad**	**10% 0.2 mrad**	**15% 0.3 mrad**
$\boldsymbol{STDF(m_0)}$	1.2	1.4	1.5	1.05	1.13	1.4
$\boldsymbol{STDF(\sigma''_{max})}$	1.07	1.13	1.2	1.02	1.04	1.08
$\boldsymbol{STDF(\rho''_{min})}$	1.05	1.12	1.2	1.02	1.04	1.09
$\boldsymbol{STDF(\varphi_{max})}$	1.06	1.11	1.2	1.02	1.04	1.08

A multilayer example

Synthetic TD and FD data generated from a three-layered model have been inverted using the CCC model and the re-parameterizations (MIC, MIR and MPA). The model was given the CCC parameters: $\sigma_0 = [50,\ 50, 50]\ mS/m$, $m_0 = [5, 300, 5]\ mV/V$, $\tau_\sigma = [0.1, 3, 5]\ s$, $C = [0.3, 0.3, 0.3]$ and thickness = [7, 7] m. The data were generated from a vertical sounding with 20 quadrupoles, with electrode spacing |AB| = 7.5 - 500 m and |MN| = 2.5 - 65 m.

The inversion results of the TD and FD data show the same features. Furthermore, the MIC, the MIR and the MPA Cole-Cole models preforms equally well. For these reasons, we only present the TD marginal posterior probability distributions of m_0 (CCC) and σ''_{max} (MIC) in Fig. 5.

The inversion results show a 3- to 6-fold improvement in the resolution from m_0 to σ''_{max} in the top and bottom layers where the chargeability is low. It is an improvement from poorly resolved parameters (Fig. 5a and Fig. 5c) to well-resolved parameters (Fig. 5d and Fig. 5f). For the remaining parameters, the differences between the two

EAGE Publications B.V., PO Box 59, 3990 DB, Houten, The Netherlands

parameterizations are negligible. In the second layer, the MIC Cole-Cole model produces a slightly lower STDF of σ''_{max} relative to m_0 (Fig. 5b and Fig. 5e), and again the differences between the parameterizations are negligible for the remaining parameters.

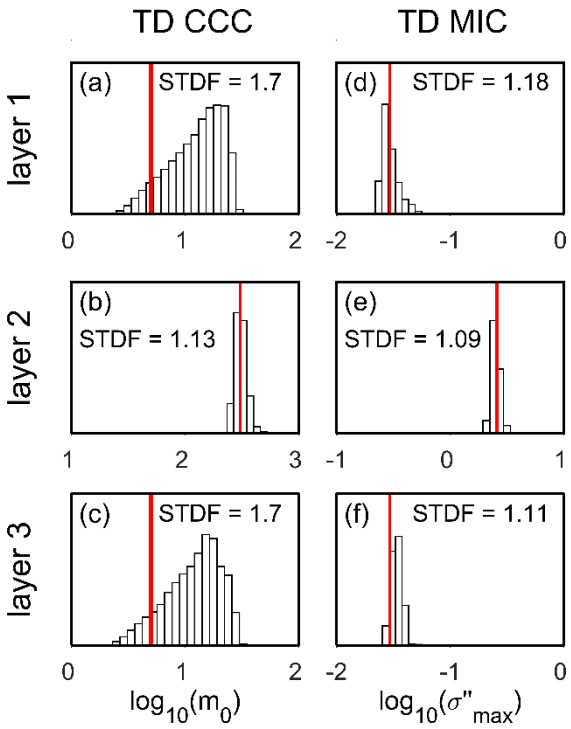

Figure 5. *Marginal posterior probability distribution and STDFs for m_0 (the conductivity Cole-Cole model) and σ''_{max} (the MIC Cole-Cole model) for the three-layer model: $\sigma_0 = [50,\ 50, 50]\ mS/m$, $m_0 = [5, 300, 5]\ mV/V$, $\tau_\sigma = [0.1, 3, 5]\ s$, $C = [0.3, 0.3, 0.3]$ and thickness = [7, 7] m. The red line marks the true model values.*

FIELD EXAMPLE

The field data were acquired at the Samsø island (Denmark). The site geology is very heterogeneous in the top 10-12 m, characterized by late-glacial meltwater deposits and

EAGE Publications B.V., PO Box 59, 3990 DB, Houten, The Netherlands

postglacial freshwater sand and peat. Below that, a clay-till layer approximately 20 m thick is present, followed by a regional aquifer in meltwater sand and gravel deposits. Below the regional aquifer, a till/clay layer is present, approximately at 40 m depth. TD IP data were collected along a 2D profile using 49 electrodes with 3 m spacing, for a total length of 144 m. The quadrupole sequence consisted of a mix of Gradient and Dipole-Dipole arrays, for a total of 1161 quadrupoles. Data were acquired using the ABEM Terrameter-LS instrument (www.guidelinegeo.com), with full-waveform signal sampled at 3750 Hz. The full-waveform signal was processed for harmonic de-noising and background drift removal following (Olsson et al., 2016) and gated using logarithmically-spaced gates from 10^{-3} to 12 s (with ten points per decade). The de-noised and re-gated TDIP data were imported to the Aarhus Workbench software (www.aarhusgeosoftware.dk) for manual processing of the IP decays. Single gates or entire decays showing poor quality, for instance due to poor signal-to-noise ratio, were removed. On average, the TD decays have 3.4 decades of usable time range after processing. A 1% standard deviation has been assigned to the resistivity data; 10% relative standard deviation plus 0.05 mV/V absolute noise has been assigned to the IP data. Vertical and horizontal constraints values, expressed as STDFs, were set up to 1.5 and 1.15, respectively.

Fig. 6 shows the inversion results for the CCC model. Panels a-d represent the uncertainty on the inversion parameters ($\sigma_0, m_0, \tau_\sigma, C$) computed following equation 22, using the final inversion model for the Jacobian computation; panels e-h show the inversion model, for the $\sigma_0, m_0, \tau_\sigma$ and C parameters. Panel i shows the data misfit. On top of the a-d and e-h panels, the DOI is shown as a black line. Fig. 7 shows the results of the MIC inversion, with uncertainty on panels a-b and model on panels e-h for the

EAGE Publications B.V., PO Box 59, 3990 DB, Houten, The Netherlands

inversion parameters $\sigma_0, \sigma''_{max}, \tau_\sigma$ and C, and misfit on panel i. On both Fig. 6 and Fig. 7 the lithological information available from a nearby borehole is superimposed on the inversion.

The σ_0, τ_σ and C inversion results are really similar in the CCC and MIC inversion of Fig. 6 and Fig. 7, both in terms of inversion model (panels e-h), uncertainty (panels a-d) and DOI. Significant differences exist between the m_0 and σ''_{max} results. The uncertainty values decrease with depth much quicker, indicating less resolution at depth. This is reflected also in the DOI estimation that is more than double for the σ''_{max} parameter. Furthermore, a better correlation between geology and σ''_{max} exists, when compared to the m_0 results. The sand layer at 4.0 m depth is better represented in the σ''_{max} section (with values below ~0.05 mS/m), with a superior thickness resolution when compared to the low-m_0 anomaly (with values below ~30 mV/V). Anomalies with high σ''_{max} values (above ~0.15 mS/m) and high m_0 values (above ~70 mV/V) correspond to the till layer (16 m thick) below 8.3 m, but the σ''_{max} anomaly resembles better the geological layer. Finally, the increase in σ''_{max} at depth correlates with the depth of the till/clay layer present below the regional aquifer, at depth of approximately 40 m.

EAGE Publications B.V., PO Box 59, 3990 DB, Houten, The Netherlands

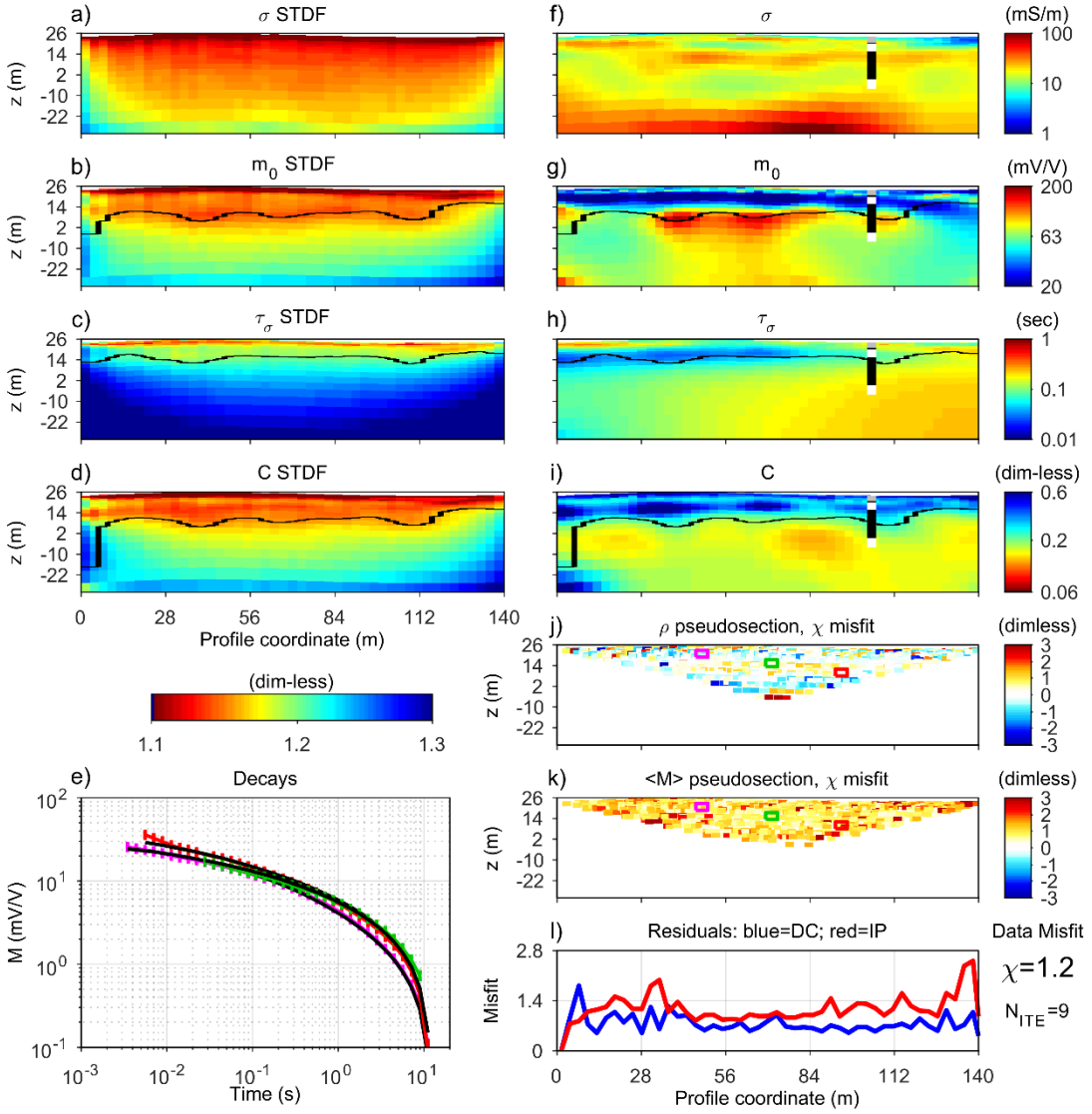

Figure 6. *Inversion model, uncertainty analysis and misfit of field data from Samsø, Denmark, obtained using the conductivity Cole-Cole parameterization. a-d) the uncertainty analysis given as the STDF of the four model parameters; e) three examples of IP decays with error bars (the locations of the data cells are marked in panel j and k) and fitting forward response (black lines); f -i) inversion model with borehole information (white is sand, black is till and grey is silt); j) resistivity pseudosection showing the misfit χ; k) pseudosection of the root mean square χ for the entire IP decay (defined positive). l) misfit of DC (blue) and IP (red) data of the inversion averaged vertically (and over all gates for the IP misfit) along the*

EAGE Publications B.V., PO Box 59, 3990 DB, Houten, The Netherlands

pseudosection. N_{ITE} is the number of iterations. The black lines in panel a-d and f-i are the DOI.

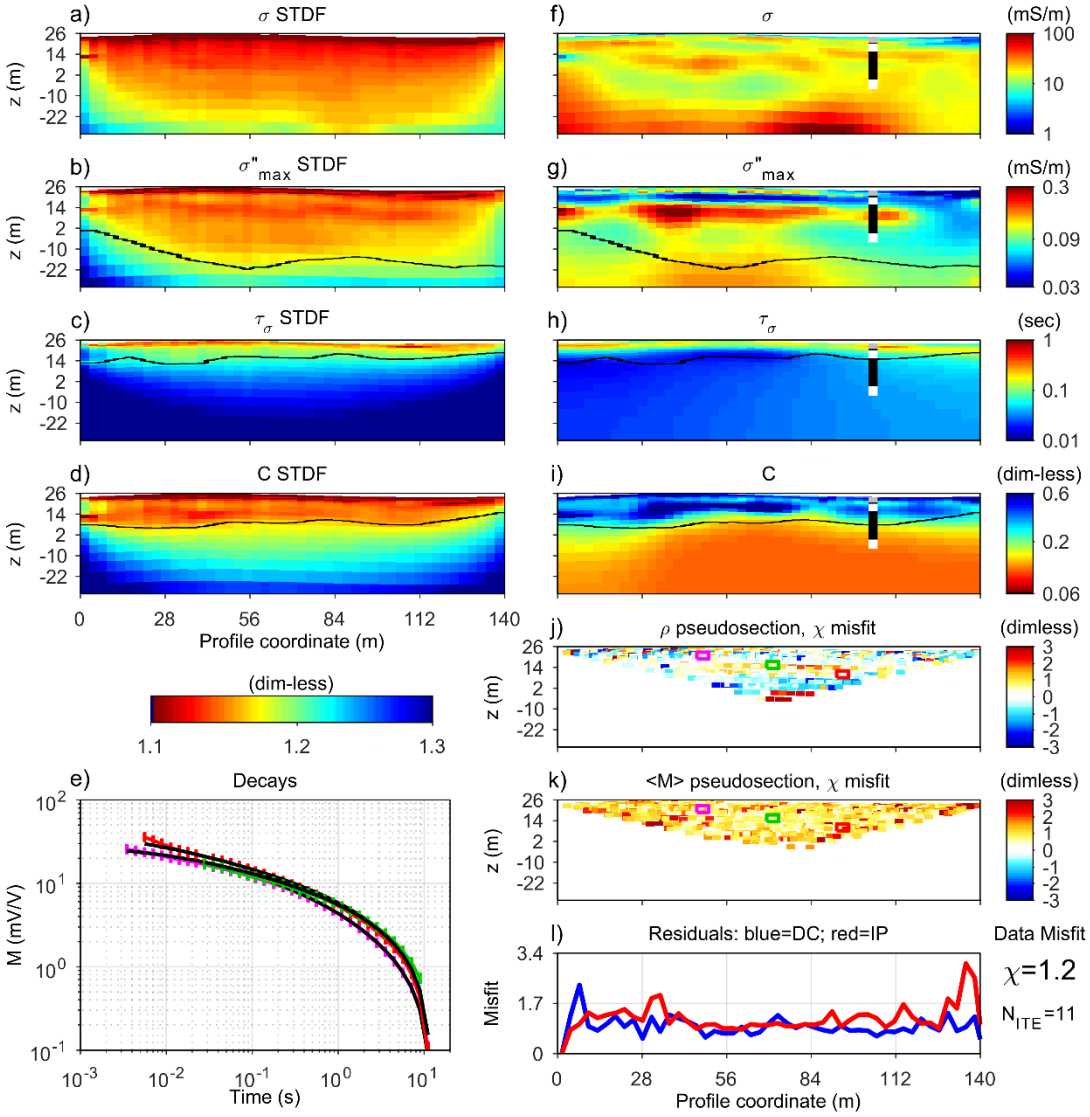

Figure 7: *Inversion model, uncertainty analysis and misfit of field data from Samsø, Denmark, obtained using the MIC Cole-Cole model for parameterization of IP. a-d) the uncertainty analysis given as the STDF of the four model parameters; e) three examples of IP decays with error bars (the locations of the data cells are marked in panel j and k) and fitting forward response (black lines); f -i) inversion model with borehole information (white is sand, black is till and grey is silt); j) resistivity*

EAGE Publications B.V., PO Box 59, 3990 DB, Houten, The Netherlands

pseudosection showing the misfit χ; k) pseudosection of the root mean square χ for the entire IP decay (defined positive). l) misfit of DC (blue) and IP (red) data of the inversion averaged vertically (and over all gates for the IP misfit) along the pseudosection. N_{ITE} is the number of iterations. The black lines in panel a-d and f-i are the DOI.

DISCUSSION

The comparison between the classic Cole-Cole model and the re-parameterizations of the Cole-Cole model has been carried out on both TD and FD IP data, but it is beyond the scope of this study to present a complete comparison of the TD and FD IP methods. In fact, the settings of the TD and FD data generation are selected focusing on getting equivalent acquisition ranges, but a TD/FD comparison study should also take other factors into account, e.g. the acquisition range actually measurable in lab/field. Despite the same number of decades (approximately 3.5 decades) being used for both TD and FD synthetic data generation, we see that the two methods are not focused at the exact same spectral range. Indeed, for $\tau = 0.1s$ (the results presented in this study), we see that the synthetic FD data often resolves the model parameters better than the TD data. However, for $\tau = 1\,s$ the situation is the opposite and the TD data gives the best resolution. With these remarks, the TD and the FD methods show approximately the same improvements with the application of the re-parameterized Cole-Cole models.

The MPA, MIC and MIR models show similar results in terms of uncertainty analysis. However, the MPA modelling has an advantage when compared to the MIC and the MIR parameterizations. Indeed, the φ_{max} parameter directly controls the magnitude of

EAGE Publications B.V., PO Box 59, 3990 DB, Houten, The Netherlands

the IP response, while in the MIC and MIR model the response magnitude depends on the σ''_{max}/σ_0 and ρ''_{min}/ρ_0 ratios, respectively.

On the other hand, many petrophysical relations involving IP properties are expressed in terms of real/imaginary conductivity, for instance the linear relation between the real and imaginary surface conductivity described in Weller et al. (2013) or the relation between hydraulic permeability and real and imaginary conductivity found by Weller et al. (2015). In this respect, the MIC model is more suited for applying petrophysical relations directly from the inversion results. A final consideration can be made about the comparison of field and laboratory IP results. Typically, laboratory IP measurements are carried out in FD, and the results are shown in terms of amplitude/phase and/or real/imaginary conductivity. In this respect, inversions of field data in terms of MPA or MIC models are much easier to compare with laboratory results in comparison to classic Cole-Cole or MIR inversions.

CONCLUSION

We have derived and tested three re-parameterization of the Cole-Cole model for inversion of TDIP and FDIP data, namely the Maximum Phase Angle (MPA) Cole-Cole model $\{\rho_0, \varphi_{\max}, \tau_\varphi, C\}$, the Maximum Imaginary Conductivity (MIC) Cole-Cole model $\{\sigma_0, \sigma''_{max}, \tau_\sigma, C\}$ and the Minimum Imaginary Resistivity (MIR) Cole-Cole model $\{\rho_0, \rho''_{min}, \tau_\rho, C\}$.

The uncertainty analyses of synthetic homogenous half space models and multilayered model, which were computed using MCMC method, show that the MPA, MIC and MIR

EAGE Publications B.V., PO Box 59, 3990 DB, Houten, The Netherlands

Cole-Cole parameters, compared to the classic Cole-Cole parameters, are less correlated in the inversion of both FD and TD IP data. Consequently, we see that the re-parameterizations increase the resolution of the model parameters, specifically of the $\varphi_{\max}$, σ''_{max} and ρ''_{min} parameters in comparison to the classic m_0 parameter. The resolution improvement obtained by the re-parameterizations is especially significant for models with low C values or low signal-to-noise ratio (i.e. models that are poorly resolved using the classic Cole-Cole model), where 3-fold improvements or better are observed. The resolution improvements are less pronounced or absent for models that are well resolved with the classic Cole-Cole model.

A 2D field example where we compare the classic Cole-Cole and the MIC models shows that gradient-based inversion methods benefit from the re-parameterizations as well. A significantly deeper (more than double) depth of investigation was found for σ''_{max} in comparison to the classic m_0, together with a better correlation with geology.

Consequently, it is recommended to invert for one of the re-parameterizations of the Cole-Cole model in any Cole-Cole inversion of IP data and then, if needed, transform the parameters back to the classic parameterization. In particular, we believe that the MPA and the MIC parameterizations will be particularly effective for the spectral inversion of field IP data and will contribute to narrow the gap between IP theory, laboratory findings and field applications.

ACKNOWLEDGMENTS

EAGE Publications B.V., PO Box 59, 3990 DB, Houten, The Netherlands

This work was cofounded by the project GEOCON (Advancing GEOlogical, geophysical and CONtaminant monitoring technologies for contaminated site investigation, www.geocon.env.dtu.dk) .

APPENDIX A

From MPA Cole-Cole to classic Cole-Cole

Given the MPA Cole-Cole model parameters $\{\rho_0, \varphi_{\max}, \tau_\varphi, C\}$, the corresponding parameters of the resistivity (or conductivity) Cole-Cole model $\{\rho_0, m_0, \tau_\rho, C\}$ can be computed through the following iterative approach.

As a start, we define the variables a and b as:

$$a(\omega) = Re\left(\frac{1}{1+(i\omega\tau_\rho)^C}\right) \quad \text{(A.1)}$$

$$b(\omega) = Im\left(\frac{1}{1+(i\omega\tau_\rho)^C}\right) \quad \text{(A.2)}$$

where Re and Im indicate the computation of the real and imaginary part of a complex number, respectively. Thus, equation 1 can be written as

$$\tilde{\rho}(\omega) = \rho_0\left[1 - m_0\left(1 - \left(a(\omega) + ib(\omega)\right)\right)\right]. \quad \text{(A.3)}$$

We now iterate to minimize

$$\Delta m_0 = \frac{|m_0(n) - m_0(n-1)|}{m_0(n)}, \quad \text{(A.4)}$$

where $m_0(0) = 0$. For the $n'th$ iteration, $\tau_\rho(n)$ and $m_0(n)$ are computed as:

$$\tau_\rho(n) = \tau_\varphi \cdot \left(1 - m_0(n-1)\right)^{-1/2C} \quad \text{(A.5)}$$

$$a(n) = Re\left(\frac{1}{1+\left(i\frac{\tau_\rho(n)}{\tau_\varphi}\right)^C}\right) \quad \text{(A.6)}$$

EAGE Publications B.V., PO Box 59, 3990 DB, Houten, The Netherlands

$$b(n) = Im\left(\frac{1}{1+\left(i\frac{\tau_\rho(n)}{\tau_\varphi}\right)^C}\right) \quad \text{(A.7)}$$

$$m_0(n) = \frac{tan(-\varphi_{max})}{(1-a(n))\cdot tan(-\varphi_{max})+b(n)}. \quad \text{(A.7)}$$

Once the classic Cole-Cole parameters $\{\rho_0, m_0, \tau_\rho, C\}$ are defined in terms of the MPA parameters $\{\rho_0, \varphi_{\max}, \tau_\varphi, C\}$, the Cole-Cole complex resistivity (or conductivity) can be computed through equation 1 (or equation 3) at any frequency.

From MIC Cole-Cole to classic Cole-Cole

Given the MIC Cole-Cole model parameters $\{\sigma_0, \sigma''_{max}, \tau_\sigma, C\}$, the corresponding parameters of the resistivity (or conductivity) Cole-Cole model $\{\rho_0, m_0, \tau_\rho, C\}$ can be computed directly.

As a start, we define the variable d as:

$$d = Im\left(\frac{1}{1+(1i)^C}\right) \quad \text{(A.8)}$$

The chargeability of the Cole-Cole model, m_0, is then given as

$$m_0 = \frac{\sigma''_{max}}{(\sigma''_{max}-\sigma_0\cdot d)}. \quad \text{(A.9)}$$

The relaxation time in the resistivity form, τ_ρ, can now be computed from equation (5)

From MIR Cole-Cole to classic Cole-Cole

Given the MIR Cole-Cole model parameters $\{\rho_0, \rho''_{min}, \tau_\rho, C\}$, the corresponding parameters of the resistivity (or conductivity) Cole-Cole model $\{\rho_0, m_0, \tau_\rho, C\}$ can be computed directly:

EAGE Publications B.V., PO Box 59, 3990 DB, Houten, The Netherlands

$$m_0 = -\frac{\rho''_{min}}{(\rho_0 \cdot d)}, \quad \text{(A.10)}$$

where d is as defined in equation A8.

APPENDIX B

Gating of TDIP signal

The gating of the transient IP signal, which is recorded from 2.6 ms to 12,000 ms, is listen in Table A.1

Table A.1: IP gating

Gate	**1**	**2**	**3**	**4**	**5**	**6**	**7**	**8**	**9**
Gate width (ms)	1.06	1.33	2.13	2.93	4	5.33	7.46	10.4	14.4
Gate	**10**	**11**	**12**	**13**	**14**	**15**	**16**	**17**	**18**
Gate width (ms)	20	20	40	60	80	100	140	200	280
Gate	**19**	**20**	**21**	**22**	**23**	**24**	**25**	**26**	
Gate width (ms)	380	540	760	1040	1460	2020	2800	2000	

Acquisition frequencies

The frequencies used for computation of synthetic frequency-domain IP forward responses.

Table A.2: Acquisition frequencies

Frequencies (Hz)												
0.08	0.16	0.32	0.64	1.28	2.56	5.12	10.2	20.4	40.9	81.9	163	327

EAGE Publications B.V., PO Box 59, 3990 DB, Houten, The Netherlands

REFERENCES

AUKEN, E., CHRISTIANSEN, A. V., JACOBSEN, B. H., FOGED, N. & SØRENSEN, K. I. 2005. Piecewise 1D Laterally Constrained Inversion of resistivity data. *Geophysical Prospecting,* 53**,** 497-506.

BÉRUBÉ, C. L., CHOUTEAU, M., SHAMSIPOUR, P., ENKIN, R. J. & OLIVO, G. R. 2017. Bayesian inference of spectral induced polarization parameters for laboratory complex resistivity measurements of rocks and soils. *Computers & Geosciences,* 105**,** 51-64.

BINLEY, A., SLATER, L. D., FUKES, M. & CASSIANI, G. 2005. Relationship between spectral induced polarization and hydraulic properties of saturated and unsaturated sandstone. *Water Resources Research,* 41**,** 1-13.

BÖRNER, F. D., SCHOPPER, J. R. & WELLER, A. 1996. Evaluation of transport and storage properties in the soil and groundwater zone from induced polarization measurements. *Geophysical Prospecting,* 44**,** 583-601.

CHEN, J., KEMNA, A. & HUBBARD, S. S. 2008. A comparison between Gauss-Newton and Markov-chain Monte Carlo-based methods for inverting spectral induced-polarization data for Cole-Cole parameters. *Geophysics,* 73**,** F247-F259.

COLE, K. S. & COLE, R. H. 1941. Dispersion and absorption in dielectrics. *Journal of Chemical Physics,* 9**,** 341-351.

FIANDACA, G., AUKEN, E., GAZOTY, A. & CHRISTIANSEN, A. V. 2012. Time-domain induced polarization: Full-decay forward modeling and 1D laterally constrained inversion of Cole-Cole parameters. *Geophysics,* 77**,** E213-E225.

FIANDACA, G., CHRISTIANSEN, A. & AUKEN, E. Depth of investigation for multi-parameters inversions. Near Surface Geoscience 2015-21st European Meeting of Environmental and Engineering Geophysics, 2015.

FIANDACA, G., RAMM, J., BINLEY, A., GAZOTY, A., CHRISTIANSEN, A. V. & AUKEN, E. 2013. Resolving spectral information from time domain induced polarization data through 2-D inversion. *Geophysical Journal International,* 192**,** 631-646.

GAZOTY, A., FIANDACA, G., PEDERSEN, J., AUKEN, E. & CHRISTIANSEN, A. V. 2012. Mapping of landfills using time-domain spectral induced polarization data: The Eskelund case study. *Near Surface Geophysics,* 10**,** 575-586.

HASTINGS, W. K. 1970. Monte Carlo sampling methods using Markov chains and their applications. *Biometrika,* 57**,** 97-109.

HÖNIG, M. & TEZKAN, B. 2007. 1D and 2D Cole-Cole-inversion of time-domain induced-polarization data. *Geophysical Prospecting,* 55**,** 117-133.

JOHANSSON, S., FIANDACA, G. & DAHLIN, T. 2015. Influence of non-aqueous phase liquid configuration on induced polarization parameters: Conceptual models applied to a time-domain field case study. *Journal of Applied Geophysics,* 123**,** 295-309.

JOHANSSON, S., SPARRENBOM, C., FIANDACA, G., LINDSKOG, A., OLSSON, P.-I., DAHLIN, T. & ROSQVIST, H. 2016. Investigations of a Cretaceous limestone with spectral induced polarization and scanning electron microscopy. *Geophysical Journal International***,** ggw432.

KEMNA, A., BINLEY, A. & SLATER, L. 2004. Crosshole IP imaging for engineering and environmental applications. *Geophysics,* 69**,** 97-107.

EAGE Publications B.V., PO Box 59, 3990 DB, Houten, The Netherlands

LEROUX, V., DAHLIN, T. & SVENSSON, M. 2007. Dense resistivity and induced polarization profiling for a landfill restoration project at Härlöv, Southern Sweden. *Waste Management & Research,* 25**,** 49-60.

LOKE, M. H., CHAMBERS, J. E. & OGILVY, R. D. 2006. Inversion of 2D spectral induced polarization imaging data. *Geophysical Prospecting,* 54**,** 287-301.

MADSEN, L. M., FIANDACA, G., AUKEN, E. & CHRISTIANSEN, A. V. 2017. Time-domain induced polarization - an analysis of Cole-Cole parameter resolution and correlation using Markov Chain Monte Carlo inversion. *Geophysical Journal International*.

MALINVERNO, A. 2002. Parsimonious Bayesian Markov chain Monte Carlo inversion in a nonlinear geophysical problem. *Geophysical Journal International,* 151**,** 675-688.

MAURYA, P. K., FIANDACA, G., AUKEN, E. & CHRISTIANSEN, A. V. Lithological characterization of a comtaminated site using direct current resistivity and time domain induced polarization. IP2016/4th International Workshop on Induced Polarization, 6.-8. June 2016 2016 Aarhus, Denmark.

METROPOLIS, N., ROSENBLUTH, A. W., ROSENBLUTH, M. N., TELLER, A. H. & TELLER, E. 1953. Equation of state calculations by fast computing machines. *The journal of chemical physics,* 21**,** 1087-1092.

MOSEGAARD, K. & TARANTOLA, A. 2002. Probabilistic Approach to Inverse Problems. *In:* W. LEE, P. J., C. KISSLINGERS, AND H. KANAMORI (ed.) *International handbook of earthquake and engineering seismology.* Academic Press.

NORDSIEK, S., DIAMANTOPOULOS, E., HÖRDT, A. & DURNER, W. 2016. Relationships between soil hydraulic parameters and induced polarization spectra. *Near Surface Geophysics,* 14**,** 23-37.

OLSSON, P.-I., FIANDACA, G., LARSEN, J. J., DAHLIN, T. & AUKEN, E. 2016. Doubling the spectrum of time-domain induced polarization by harmonic de-noising, drift correction, spike removal, tapered gating and data uncertainty estimation. *Geophysical Journal International,* 207**,** 774-784.

OLSSON, P. I., DAHLIN, T., FIANDACA, G. & AUKEN, E. 2015. Measuring time-domain spectral induced polarization in the on-time:decreasing acquisition time and increasing signal-to-noise ratio. *Journal of Applied Geophysics,* 2015**,** 6.

PELTON, W. H., WARD, S. H., HALLOF, P. G., SILL, W. R. & NELSON, P. H. 1978. Mineral discrimination and removal of inductive coupling with multifrequency IP. *Geophysics,* 43**,** 588-609.

SEIGEL, H. O. 1959. Mathematical Formulation and type curves for induced polarization. *Geophysics,* 24**,** 547-565.

SLATER, L. D. & LESMES, D. 2002. IP interpretation in environmental investigations. *Geophysics,* 67**,** 77-88.

TARASOV, A. & TITOV, K. 2013. On the use of the Cole–Cole equations in spectral induced polarization. *Geophysical Journal International,* 195**,** 352-356.

VANHALA, H. 1997. Mapping oil-contaminated sand and till with the spectral induced polarization (IP) method. *Geophysical Prospecting,* 45**,** 303-326.

WELLER, A., SLATER, L., BINLEY, A., NORDSIEK, S. & XU, S. 2015. Permeability prediction based on induced polarization: Insights from measurements on sandstone and unconsolidated samples spanning a wide permeability range. *Geophysics,* 80**,** D161-D173.

WELLER, A., SLATER, L. & NORDSIEK, S. 2013. On the relationship between induced polarization and surface conductivity: Implications for petrophysical interpretation of electrical measurements. *Geophysics,* 78**,** D315-D325.

YOSHIOKA, K. & ZHDANOV, M. S. 2005. Three-dimensional nonlinear regularized inversion of the induced polarization data based on the Cole-Cole model. *Physics of the Earth and Planetary Interiors,* 150**,** 29-43.

YUVAL & OLDENBURG, D. W. 1997. Computation of Cole-Cole parameters from IP data. *Geophysics,* 62**,** 436-448.

Reviewer 1:

The authors confirmed with their modeling studies the well-known fact from previous publications that the Cole-Cole-parameters (unfortunately, they show here only the chargeability) can only be resolved if m>0.3 (see, for example, the 1D modeling study on page 69). However, this fact is not really mentioned throughout the paper. A better resolution of the model parameters with small values can be obtained by the re-parametrization and this is an interesting result of this study.
We disagree on the fact that only m0>0.3 (V/V) can be resolved. In figure 5, the three layers model, we have 5, 300 and 5 mV/V for m0. The second layer is resolved better than the first and third in the classic Cole-Cole inversion (but also in the MIC), with m0 poorly resolved in the first and third layers. But many models with m0 values between 5 and 300 mV/V can be resolved, even if it is not shown in the paper. And the STDF on the model space depends on the data errors.

No re-parametrization is necessary for a large m and this should clearly be mentioned.
We state that "the increase in model resolution is particularly significant for models that are poorly resolved using the classic cole-cole parameterization, for instance for low values of the frequency exponent or low signal to noise ratio". The small m0 values often gives small S/N, but this depends on the standard deviation of the data. So we retain that our way of presenting the results in the manuscripts describes correctly what was found.

General statements should be avoided. For example abstract on page 47: "the reparametrization lead significantly deeper depth of investigation" .It can depend on the model parameters and the subsurface structure.
Yes it does. But almost always there is a significant improvement. We modified the sentence into: "In general, this leads to a significantly deeper depth of investigation…"

The reference to Mauraya et al 2017 is not complete in the reference list.
Thanks, the reference has been updated.

The authors varied c to study the resolution of the model parameters. I would vary m and study the resolution. Instead, they varied the signal to noise ratio.
We think that this is the most appropriate way to do it, because it's the signal to noise ratio that drives the m0 resolution, and not the m0 value itself (even if this means that high m0 values give good resolution).

Reference model in Fig 1: m=100 mV/V and in Fig. 2 m=500 mV/V. Please check.
Yes, It is 500 mV/V in fig 1 and 100 mV/V in fig 2. As we understand that this might bring confusion, we added the sentence:
"The high m_0-value was chosen to emphasize the frequency variation of the spectrum."

How do you calculate STFD if you have negative IP data? Instead of a logarithmic transformation, another type of transformation could be used (for example asinhtransformation).

The logarithmic transformation for the data is performed only when no negative data are present. In any case, the STDF on the model parameters can be computed both with the linear and logarithmic data transformation, and it is not affected by it in the MCMC inversion.
For clearification we change on page 12-13 (eq. 14):
"$d_{obs}=\{\rho_a, M_i\}, i=1:N\_gates$ (14)
where … If no negative data are present, the inversion is performed in the logarithmic space."

It seems to me as if the authors regard MCMC as the only technique to examine the resolution of model parameters (page 58). But a good resolution can also be achieved by using the SVDanalysis.
We added on page 14 (58 in the reviewer's document):
"(as well as other statistical inversion approaches)"

k is not defined in Eq. 17
Thank you, it has now been stated that it is a normalization constant.

What is the reason for assuming STDF=4? (page 62)
We added to the text:
"Based on experience, DOI threshold values between 2 and 5 gives reasonable DOI estimations. The values of the DOI threshold are usually increased for the τ parameter, which is significantly less resolved and for which the order of magnitude is of interest even when the parameter resolution is low. In this study, the DOI threshold is STDF = 4 for all parameter except τ, for which STDF = 20."

Homogenous half space example: On page 63: m=200 mV/v, but in the caption of Fig. 3 you wrote: m=100 mV/V. Which value is the correct one?
Thank you, this is a misprint. The correct value is m0=100 mV/V. This has been corrected.

I am wondering why the conductivity in Fig. 2a has a relative large model space? Do you have an explanation?
Sorry, we did not understand the comment. In fig 2a we show the data space phase as function of frequency.

Changing the noise model: Only m is considered. What happened with the other Cole-Cole parameters?
For a more through description, we have added the following to page 23 "Changing the noise model" section:
"For all parameterizations, we see that as the noise level is increases, the STDF of the model parameters increases as well. This is also valid for the parameters not shown in the table."
"As seen with the example in Fig. 3, the resolution improvement gained with the re-parameterizations is less pronounced for the remaining parameters."

I thank the authors that they also considered a multilayer case. But again, only m is considered in this example. The model has many other model parameters including the remaining Cole parameters and the thickness of the layer. My experience is, for example, that the thickness

of the layer is also very important for the resolution of all model parameters. This fact should be considered and clearly shown in the paper.
We have added some more information about the other parameters to the section "A multilayer example".

"… in the top and bottom layers where the chargeability is low… For the remaining parameters the differences between the two parameterizations are negligible. In the second layer, the MIC Cole-Cole model produces a slightly lower STDF of σ_{max}'' relative to m_0 (Fig. 5b and Fig. 5e), and again the differences between the parameterizations are negligible for the remaining parameters."

Thank you for also considering a field example. Here again, I would avoid strong statements about the re-parametrization and that it would fit better to the geology. Both modeling results would - in terms of equivalent models – confirm the borehole result. The data of two selected stations and their model fittings can be shown using both approaches.
We changed the figures including data and forward responses for selected quadrupoles.

Reviewer 2:

p13: form 2.6ms -> from 2.6ms

Thank you, we have corrected the misprint.